Vortex-lattice melting in two-dimensional superconducting networks and films

M. Franz and S. Teitel
Department of Physics and Astronomy, University of Rochester, Rochester, New York 14627
(Received 2 September 1994)

We carry out an extensive Monte Carlo study of phase transitions in two-dimensional (2D) superconducting networks, in an applied magnetic field, for square and honeycomb geometries. We consider both systems with a dilute vortex density $1/q$, and dense systems near full frustration with vortex density $1/2$–$1/q$. The dilute case gives the continuum limit as $q \to \infty$, and serves as a model for a uniform superconducting film. For this dilute case, we find a transition temperature $T_c \sim 1/q$, at which the vortex lattice unpins from the network and forms a "floating solid" phase. At a higher temperature T_m, this floating solid melts into a vortex liquid. We analyze the transition at T_m according to the Kosterlitz-Thouless theory of dislocation mediated melting in 2D. While we find a discontinuous jump in the vortex shear modulus at T_m which is consistent with this theory, we find (in opposition to this theory) that the transition is weakly first order, and we find no evidence for a hexatic liquid phase. For the case near full frustration, we find that the system can be described in terms of the density of defects in an otherwise fully frustrated vortex pattern. These dilute defects result in similar behavior as that found in the dilute vortex system, with pinned, floating, and liquid defect phases.

I. INTRODUCTION

Two-dimensional (2D) periodic superconducting networks, and in particular arrays of Josephson junctions, have served as a convenient theoretical and experimental model system in terms of which one can study, in a well-controlled way, the effects of thermal fluctuations and pinning, on vortex structures and phase coherence in 2D superconductors.[1] Such 2D superconductors have received renewed attention recently with the observation that many of the high-temperature superconductors consist of weakly coupled layers, and so for some range of parameters may display effectively two dimensional behavior.[2,3] One focus of this renewed interest has been concerned with the melting of the 2D vortex lattice, induced by an applied magnetic field, in a uniform continuous superconducting film. Controversy has resulted as to whether such a vortex lattice even exists at any finite temperature, or whether a vortex liquid is the only thermodynamically stable state.[4] In this work we address the thermodynamic behavior of vortex structures in 2D superconducting systems. Our focus will be on their behavior in discrete periodic networks; however, our results will also yield conclusions concerning the behavior of uniform films.

Despite a decade of theoretical work, many fundamental questions remain unresolved concerning the nature of the phase transitions in 2D superconducting networks. When a uniform transverse magnetic field is applied, it induces a fixed density of vortices into the network, as in the mixed state of a type-II superconductor. However, unlike a uniform superconductor, for which the ground state is a periodic triangular lattice of equally spaced vortices, the discrete network structure serves as an effective periodic pinning potential, which at low temperatures confines the vortices to sit at the centers of the unit cells of the network. This can result in novel vortex structures at low temperature, determined by the competition between the repulsive vortex-vortex interaction, and the periodic pinning potential induced by the network.[5–7] Finding the ground state vortex structure for an arbitrary value of vortex density, for a given periodic network, remains an unsolved problem. The phase transitions at finite temperature have remained largely unexplored except for a few of the simplest cases.[8–11]

An early conjecture by Teitel and Jayaprakash[5] (TJ) argued that the superconducting transition in such networks would be governed by commensurability effects. If one measures the dimensionless vortex density f as the number of magnetic-field-induced vortices per unit cell of the network, they predicted that for rational $f = p/q$, the transition temperature would vary discontinuously as $T_c(p/q) \sim 1/q$. While experimental evidence for high-order commensurability effects has been reported in Josephson junction arrays,[12] simulations by Halsey[13] have challenged this conjecture for large q. A similar conjecture by TJ (Ref. 5) concerning the behavior of the ground state critical current $i_c(f)$ has since been disproved in simulations by Lobb and co-workers,[14,15] and by Straley,[16] who argue that as f varies, $i_c(f)$ has a lower nonzero limit determined by the single-body effects of a noninteracting vortex in a periodic pinning potential; this conclusion has also been arrived at analytically by Vallat and Beck.[17] However, the validity of the TJ conjecture with respect to $T_c(f)$, which is intrinsically determined by many-body effects, has remained unresolved.[18]

In this paper we attempt to study the TJ conjecture systematically, by carrying out Monte Carlo (MC) simulations of superconducting networks for two special classes of vortex density. We first consider the dilute case

0163-1829/95/51(10)/6551(24)/$06.00

of vortex densities $f = 1/q$, q integer, for both square and honeycomb networks. This dilute case, as $q \to \infty$, can equivalently be viewed as the continuum limit, in which the lattice spacing of the periodic network decreases to zero for a fixed areal density of vortices. Our results for this case therefore also address the problem of vortex-lattice melting in a uniform continuous superconducting film. Second, we consider vortex densities $f = 1/2 - 1/q$, close to full frustration, on the square network.

Our results may be summarized as follows. For the dilute case with large q, the low-temperature state is a Bravais lattice of vortices, with long-range translational order, pinned commensurably to the periodic network. At a critical temperature $T_c(1/q) \sim 1/q$, there is a sharp first-order phase transition to a floating triangular vortex lattice, which is depinned from the periodic potential of the network. This floating lattice displays the algebraic translational correlations characteristic of a 2D vortex lattice in a uniform continuum. The depinning transition $T_c(f)$ satisfies the TJ conjecture, and marks the loss of true dc superconductivity in the network, due to the flux flow resistance which will result from drift of the unpinned vortex lattice. At a higher T_m, which becomes independent of q as $1/q \to 0$, this floating vortex lattice melts into an isotropic vortex liquid. We analyze this transition according to the theory of dislocation-mediated melting in 2D, due to Kosterlitz and Thouless (KT),[19] Nelson and Halperin,[20] and Young[21] (KTNHY). While we find good agreement with certain predictions of this KTNHY theory, we find evidence that the second-order melting transition predicted by KTNHY is preempted by a weak first-order transition.

For the close to fully frustrated case, $f = 1/2 - 1/q$, the ground state is everywhere like that of $f = 1/2$ (a checkerboard pattern of vortices on alternating sites), except for a superimposed commensurate Bravais lattice of missing vortices, or "defects," so as to give the desired density $f < 1/2$. The transitions in this system are then governed by the behavior of these defects. Upon heating, there is first a depinning transition $T_c(f)$ of the defect Bravais lattice into a floating triangular defect lattice; this depinning follows the TJ conjecture, $T_c(f) \sim 1/q$, and marks the loss of true dc superconductivity. At a higher T_m, the floating defect lattice melts into an isotropic defect liquid. Finally, at a higher $T_{m'}$, there is an additional sharp transition representing the disordering of the vortices forming the $f = 1/2$ like background.

The remainder of our paper is organized as follows. In Sec. II we present the theoretical model used to describe the superconducting network, and its relation to a uniform superconducting film. We review the KTNHY theory of 2D melting, and discuss the observables we measure and the methods we use to analyze our data. Finally we describe our Monte Carlo procedure. In Sec. III we present our results for the dilute case $f = 1/q$ on a honeycomb network. This corresponds to vortices on the dual triangular lattice of sites. We use finite-size scaling to test in detail the predictions of KTNHY. In Sec. IV we present our results for the dilute case $f = 1/q$ on a square network. In Sec. V we present our results for the dense case of $f = 5/11$ on a square lattice, and infer the behavior for more general densities $f = 1/2 - 1/q$. In Sec. VI we present our discussion and conclusions.

II. MODEL AND METHODS OF ANALYSIS

A. Model for a superconducting network

A two-dimensional superconducting network in a magnetic field is described by the Hamiltonian

$$\mathcal{H}[\theta_i] = \sum_{\langle ij \rangle} U(\theta_i - \theta_j - A_{ij}) , \tag{1}$$

where θ_i is the fluctuating phase of the superconducting wave function on node i of a periodic network of sites. The sum is over pairs of nearest neighbor sites, representing the bonds of the network, and

$$A_{ij} = (2\pi/\Phi_0) \int_i^j \mathbf{A} \cdot d\mathbf{l} \tag{2}$$

are fixed constants, giving the integral of the magnetic vector potential across bond $\langle ij \rangle$ ($\Phi_0 = hc/2e$ is the magnetic flux quantum). $U(\theta)$ is the interaction potential between neighboring nodes, and its argument is just the gauge-invariant phase difference across the bond. $U(\theta)$ is periodic in θ with period 2π, and has its minimum at $\theta = 0$. We will be interested here in the case of a uniform applied magnetic field $\nabla \times \mathbf{A} = \mathbf{B}$, transverse to the plane of the network. In this case, the sum of the A_{ij} going counterclockwise around any unit cell of the network is constant, and determined by the magnetic flux through the cell,

$$\sum_{\text{cell}} A_{ij} = 2\pi \mathcal{A} B/\Phi_0 \equiv 2\pi f, \tag{3}$$

where $\mathcal{A}$ is the area of a unit cell of the network. f therefore is the number of flux quanta of applied magnetic field, per unit cell.

For an array of Josephson junctions, the interaction potential in Eq. (1) is taken as $U(\theta) = -J_0 \cos(\theta)$. For a superconducting wire network, in the London approximation, a more appropriate interaction[22] is given by the Villain function,[23] defined by

$$e^{-U(\theta)/T} \equiv \sum_{m=-\infty}^{\infty} e^{-J_0(\theta - 2\pi m)^2/2T} , \tag{4}$$

where we take $k_B \equiv 1$.

For the Villain interaction, one can show by duality transformation[24] that the Hamiltonian of Eq. (1) can be mapped onto the 2D classical Coulomb gas

$$\mathcal{H} = \frac{1}{2} \sum_{ij} (n_i - f) V(\mathbf{r}_i - \mathbf{r}_j)(n_j - f), \tag{5}$$

where the sum is over all sites i, j of the *dual* lattice of the periodic network [i.e., the sites i in Eq. (5) lie at the centers of the unit cells of the network]. $n_i = 0, \pm 1, \pm 2, \ldots$ are integer "charges" representing vortices in the phases

θ_i, and the magnetic field flux density is represented by the uniform background charge $-f$. $V(\mathbf{r})$ is the lattice Coulomb potential in 2D, which solves the equation

$$\Delta^2 V(\mathbf{r}) = -2\pi\delta_{\mathbf{r},\mathbf{0}}, \tag{6}$$

where Δ^2 is the discrete Laplacian for the network. For large separations, $V(\mathbf{r}) \simeq \ln|\mathbf{r}|$. In mapping from the network Hamiltonian given by Eqs. (1) and (4), to the Coulomb gas Hamiltonian of Eq. (5), we have followed convention[25] by rescaling the temperatures so that $T_{\rm CG} = T_{XY}/2\pi J_0$, where $T_{\rm CG}$ refers to the temperature in the Coulomb gas model, and T_{XY} refers to the temperature in the network (also referred to as a "uniformly frustrated" XY model[5]). Henceforth, we will denote $T_{\rm CG}$ as simply T.

Our simulations will be carried out in terms of this Coulomb gas problem, rather than in terms of the phases θ_i. Although the Villain interaction may give quantitative differences when compared to the cosine interaction of a Josephson array, since the two functions have the same symmetry, we expect that they will display the same qualitative critical behavior.[26]

For our simulations, we work with a finite $L \times L$ grid of sites, and apply periodic boundary conditions to the Laplacian, Eq. (6), defining the Coulomb potential $V(\mathbf{r})$. In this case, V can be explicitly calculated in terms of its Fourier transform.[11] For a square network of lattice constant a_0, one finds

$$V(\mathbf{r}) = \frac{\pi}{N}\sum_{\mathbf{k}} \frac{e^{i\mathbf{k}\cdot\mathbf{r}}}{2-\cos(\mathbf{k}\cdot\mathbf{a}_1)-\cos(\mathbf{k}\cdot\mathbf{a}_2)}, \tag{7}$$

where $N = L^2$, $\{\mathbf{a}_1,\mathbf{a}_2\} = \{a_0\hat{\mathbf{x}}, a_0\hat{\mathbf{y}}\}$ are the basis vectors, and the summation is over all wave vectors consistent with the periodic boundary conditions, i.e., the set $\{\mathbf{k}\} = \{(m_1/L)\mathbf{b}_1 + (m_2/L)\mathbf{b}_2\}$, with $m_1, m_2 = 0, 1, 2 \ldots L-1$, and with $\{\mathbf{b}_1,\mathbf{b}_2\} = \{(2\pi/a_0)\hat{\mathbf{x}}, (2\pi/a_0)\hat{\mathbf{y}}\}$ the basis vectors of the reciprocal lattice.

For a honeycomb network, the charges n_i sit on the dual triangular grid of sites, and the Coulomb potential is given by[56]

$$V(\mathbf{r}) = \frac{3\pi}{2N}\sum_{\mathbf{k}} \frac{e^{i\mathbf{k}\cdot\mathbf{r}}}{3-\cos(\mathbf{k}\cdot\mathbf{a}_1)-\cos(\mathbf{k}\cdot\mathbf{a}_2)-\cos(\mathbf{k}\cdot\mathbf{a}_3)}, \tag{8}$$

where $\{\mathbf{a}_1,\mathbf{a}_2\} = \{a_0\hat{\mathbf{x}}, a_0(\hat{\mathbf{x}}/2 + \sqrt{3}\hat{\mathbf{y}}/2)\}$ are the basis vectors, $\mathbf{a}_3 = \mathbf{a}_2 - \mathbf{a}_1$, and the wave vectors are determined by $\{\mathbf{b}_1,\mathbf{b}_2\} = \{(2\pi/a_0)[\hat{\mathbf{x}} - (1/\sqrt{3})\hat{\mathbf{y}}], (2\pi/a_0)(2/\sqrt{3})\hat{\mathbf{y}}\}$.

The $\mathbf{k} = 0$ terms in the summations of Eqs. (7) and (8) will cause a divergence in $V(\mathbf{r})$. In real space, this is a reflection of the infinite self-energy of a point charge. Configurations with infinite total energy will carry zero weight in the partition function sum, and may therefore be excluded. To keep the energy of the Coulomb gas finite, we therefore impose the condition of overall charge neutrality

$$\sum_i (n_i - f) = 0. \tag{9}$$

If we define N_c as the total number of charges in the system, then Eq. (9) gives

$$N_c \equiv \sum_i n_i = fN. \tag{10}$$

Thus the density of magnetic flux quanta f is equal to the density of charges (vortices) N_c/N. In the neutral system, the infinite self-energies will exactly cancel, and in place of $V(\mathbf{r})$ we can use only the nonsingular part of the Coulomb potential (7) and (8) defined by $V'(\mathbf{r}) \equiv V(\mathbf{r}) - V(\mathbf{r}=0)$. For a given system size, we evaluate $V'(\mathbf{r})$ by numerically performing the summations indicated in Eqs. (7) and (8).

The ground state will therefore be a periodic vortex structure consisting of N_c sites with $n_i = +1$ (all other sites having $n_i = 0$), spaced as equally apart as allowed by the network geometry. Understanding the behavior of this vortex structure at finite temperature will be one of the main goals of this work.

B. Relation to a uniform superconducting film

The Coulomb gas model of the preceding section can also be used to describe the melting of the vortex lattice in a uniform continuous superconducting film. For a superconducting film, the states of the system can be described by a complex wave function, $\psi(\mathbf{r}) = |\psi(\mathbf{r})|e^{i\theta(\mathbf{r})}$. As shown by Pearl,[28] for a of film of thickness d, provided the sample size is smaller than the transverse magnetic penetration length $\lambda_\perp = \lambda^2/d$, the magnetic field will be essentially uniform and constant throughout the film. In this case, the states $\psi(\mathbf{r})$ will be weighted in the partition function sum according to the Ginzburg-Landau free energy

$$\mathcal{H}_{\rm GL}[\psi] = \int d^2r \left\{ \alpha|\psi|^2 + \frac{1}{2}\beta|\psi|^4 + \frac{1}{2m}\left|\left(\frac{\hbar}{i}\nabla - \frac{2e}{c}\mathbf{A}\right)\psi\right|^2 \right\}, \tag{11}$$

with $\nabla\times\mathbf{A} = \mathbf{B}$ a fixed constant. The mean field solution that minimizes $\mathcal{H}_{\rm GL}[\psi]$ is similar to that found[29] in three dimensions: (i) There is a triangular lattice of equally spaced vortices in the phase $\theta(\mathbf{r})$; (ii) the areal density of vortices is B/Φ_0, with an average separation of $a_v \sim \sqrt{\Phi_0/B}$; (iii) the size of the normal core of a vortex is determined by $\xi_0 \sim 1/\sqrt{\alpha}$, where $\alpha = 0$ determines the $B = 0$ mean field transition temperature; and (iv) the mean field phase transition at finite B occurs when $\xi_0 \sim a_v$.

To include fluctuations, one should now sum the partition function over all fluctuations of $\psi(\mathbf{r})$ about the mean field solution. In doing so, one common approach has been to make the London approximation. Here one assumes that, outside of the normal vortex core, the amplitude of the superconducting wave function is kept con-

stant, and only the phase fluctuates, i.e., $\psi(\mathbf{r}) = |\psi|e^{i\theta(\mathbf{r})}$. The London approximation is expected to be good whenever the bare vortex core radius is very much smaller than the average separation between vortices, $\xi_0 \ll a_v$; by (iv) above, this corresponds to temperatures well below the mean field phase transition.

Substituting $\psi(\mathbf{r}) = |\psi|e^{i\theta(\mathbf{r})}$ into Eq. (11) results, within additive constants, in the simplified free energy

$$\mathcal{H}[\theta] = \frac{1}{2}J_0 \int d^2r \left|\nabla\theta - \frac{2\pi}{\Phi_0}\mathbf{A}\right|^2, \tag{12}$$

where $J_0 = \Phi_0^2/16\pi^3\lambda_\perp$, and the integral is implicitly cut off at the vortex cores. Equation (12) is just a continuum version of the network Hamiltonian, Eq. (1). Following Halperin and Nelson[30] who considered the $B = 0$ case, and Huberman and Doniach[31] and Fisher[32] who considered the finite-B case, we note that Eq. (12) can be mapped onto a continuum Coulomb gas of logarithmically interacting charges. For finite B, this can be written[25] in the form of a one-component plasma on a uniform background charge density B/Φ_0,

$$\mathcal{H} = \frac{1}{2}\int d^2r d^2r' [n(\mathbf{r}) - B/\Phi_0]V(\mathbf{r}-\mathbf{r}')[n(\mathbf{r}') - B/\Phi_0]. \tag{13}$$

Here $n(\mathbf{r}) \equiv (1/2\pi)\hat{\mathbf{z}}\cdot\nabla\times\nabla\theta$ is the vorticity in the phase of the superconducting wave function, determined by singular integer vortices n_i at positions $\mathbf{r}_i$, $n(\mathbf{r}) = \sum_i n_i\delta(\mathbf{r}-\mathbf{r}_i)$. $V(\mathbf{r})$ solves the 2D Laplace equation, $\nabla^2 V = -2\pi\delta(\mathbf{r})$.

The Coulomb gas of Eq. (5), introduced in the preceding section as a description for a network, can now be viewed as a discrete approximation to the continuum problem of Eq. (13). For a fixed areal density of vortices, B/Φ_0, we recover the continuum equation (13) from the discrete equation (5) as we take the network lattice constant $a_0 \to 0$. Since the number of vortices per unit cell in the network is $f \sim a_0^2 B/\Phi_0$, we see that the continuum is equivalent to the $f \to 0$ limit. Thus by studying the melting of dilute vortex lattices in a network, we can also learn about the melting of a vortex lattice in a uniform superconducting film. As in the previous section, the mapping between the Coulomb gas and the superconductor is obtained by measuring the Coulomb gas temperature $T_{\rm CG}$ in units of $2\pi J_0 = \Phi_0^2/8\pi^2\lambda_\perp$, i.e., $T_{\rm super} = 2\pi J_0 T_{\rm CG}$.

Finally, we note that the melting of the 2D vortex lattice, described by the continuum Coulomb gas Hamiltonian of Eq. (13), has been treated within the general 2D melting theory of KTNHY. Within this theory, Fisher[32] has estimated that the melting transition occurs more than an order of magnitude below the mean field transition. This observation completes the self-consistency of the argument for using the London approximation.

C. Review of the theory of 2D melting

The analysis of our results will be guided by the ideas of the theory of defect-mediated melting in 2D, developed by KTNHY.[19–21] Although our results are, in many aspects, in opposition to this KTNHY theory, it still represents a useful starting point in exploring the phenomenon of 2D melting.

For the 2D harmonic crystal on a smooth substrate (i.e., in the absence of any one-body potential) it is well known that fluctuations in the long-wavelength phonon modes lead to a logarithmic divergence in the displacements of the particles, destroying translational long-range order at any finite temperature. This is a consequence of the rigorous Mermin-Wagner theorem[33] concerning long-range order in 2D. The standard theory of elasticity shows, however, that despite the absence of translational long-range order, the low-temperature phase of such a crystal is characterized by a slow power-law decay of translational correlations,[34,35] very different from the fast exponential decay that one would expect in the liquid. This phenomenon has been termed "quasi-long-range" order, and we shall refer to such a phase as a "2D solid." Based on the ideas of Kosterlitz and Thouless,[19] that the melting of such a 2D solid would be nucleated by the unbinding of topological lattice defects, Nelson and Halperin[20] and Young[21] formulated a theory (KTNHY) which predicted that 2D melting would occur via two separate second-order KT-like transitions. In particular, they predicted that the 2D solid with algebraic translational correlations would become unstable to the unbinding of dislocation defect pairs at a temperature T_m, and melt into a new phase called the hexatic liquid. This hexatic phase would be characterized by short-range translational order, but quasi-long-range sixfold orientational order. As the temperature is increased, KTNHY predicted that this quasi-long-range orientational order would eventually be destroyed by the unbinding of disclination defect pairs, and at $T_i > T_m$, the hexatic liquid would melt into a normal (isotropic) liquid with short-range orientational order. We summarize this scenario by writing down the long-range limiting behavior predicted for the translational and orientational correlation functions.

For translational correlations,

$$\langle e^{i\mathbf{G}\cdot(\mathbf{r}_i-\mathbf{r}_j)}\rangle \sim \begin{cases} 1 & \text{in perfect crystal } (T=0), \\ r_{ij}^{-\eta_{\mathbf{G}}(T)} & \text{in 2D solid } (0<T<T_m), \\ e^{-r_{ij}/\xi_+} & \text{in hexatic or normal liquid } (T>T_m), \end{cases} \tag{14}$$

where $r_{ij} = |\mathbf{r}_i - \mathbf{r}_j|$ is the separation between particles i and j, and $\mathbf{G}$ is a reciprocal lattice vector of the perfect (triangular) crystal at $T = 0$. $\eta_{\mathbf{G}}(T)$ is a temperature-dependent exponent, which for the 2D harmonic crystal can be expressed in terms its shear modulus μ and bulk modulus λ as

$$\eta_{\mathbf{G}}(T) = \frac{k_B T|\mathbf{G}|^2(3\mu+\lambda)}{4\pi\mu(2\mu+\lambda)}. \tag{15}$$

In the 2D vortex lattice, the bulk modulus λ is infinite because of the long-ranged nature of the Coulomb interaction. The expression for $\eta_{\mathbf{G}}(T)$ thus simplifies to

$$\eta_{\mathbf{G}}(T) = \frac{k_B T |\mathbf{G}|^2}{4\pi\mu}. \tag{16}$$

A key prediction of the KTNHY theory is that if $\mathbf{G}_1$ is a shortest reciprocal lattice vector, then $\eta_{\mathbf{G}_1}^{-1}(T)$ takes a discontinuous jump at T_m to zero from the universal value

$$\eta_{\mathbf{G}_1}^{-1}(T_m^-) = 3. \tag{17}$$

In what follows, we will directly test this prediction. We wish to stress, however, that the behavior of translational correlations in the 2D solid phase, as given by Eq. (14), is a general result of continuum elastic theory, independent of all assumptions concerning the mechanism of the melting transition. It is only the universal jump in $\eta_{\mathbf{G}_1}^{-1}(T_m)$, and the existence of the hexatic phase, which are specific predictions of KTNHY.

The sixfold orientational correlation function, according to KTNHY, behaves as

$$\langle e^{6i[\vartheta(\mathbf{r}_i)-\vartheta(\mathbf{r}_j)]}\rangle \sim \begin{cases} \alpha e^{-r_{ij}/\xi_6'} + \varphi_6^\infty & \text{in 2D solid } (0 < T < T_m), \\ r_{ij}^{-\eta_6(T)} & \text{in hexatic liquid } (T_m < T < T_i), \\ e^{-r_{ij}/\xi_6} & \text{in normal liquid } (T > T_i), \end{cases} \tag{18}$$

where $\vartheta(\mathbf{r}_i)$ is the angle of the bond from particle i to its nearest neighbor, relative to some fixed reference direction. α is a proportionality constant of order 1, and φ_6^∞ gives the value of the long-range orientational order expected in the 2D solid phase. The exponent $\eta_6^{-1}(T)$, describing the quasi-long-range order of the hexatic phase, is predicted to have a universal jump to zero at T_i from the value $\eta_6^{-1}(T_i^-) = 4$.

In the 2D solid, a relation between φ_6^∞ and the vortex shear modulus μ can be derived from continuum elastic theory,[35]

$$\varphi_6^\infty \simeq \exp\left[-\frac{9k_BT\Lambda^2}{8\pi\mu}\right] = \exp\left[-\frac{9\Lambda^2\eta_{\mathbf{G}}}{2|\mathbf{G}|^2}\right], \tag{19}$$

where $\Lambda \sim 2\pi/a_v$ is an ultraviolet cutoff (a_v is the average separation between particles). Since we will independently measure φ_6^∞ and $\eta_{\mathbf{G}}$ in our simulation, we will use this relation as a check of the consistency of our results.

For a periodic superconducting network, we have discussed how the discrete substrate of the network serves to induce a periodic pinning potential for the magnetic-field-induced vortices. To treat this case, we are therefore interested in how the above 2D melting scenario is altered by the presence of a periodic substrate. We shall be interested in the situation where the period of the substrate is sufficiently small compared to the spacing between particles, so that the essential features of the defect-mediated melting theory remain intact. This problem has been treated by Nelson and Halperin.[20] The main result of such a "fine-mesh" periodic perturbation is the appearance of a new phase at low temperatures, in which the 2D solid is commensurably pinned to the substrate. This phase has true long-range translational order, and we shall refer to it as the "pinned solid." At a certain depinning temperature $T_c < T_m$, there is a transition to a 2D "floating solid" phase, where the solid decouples from the substrate, and translational correlations behave identically to those of a 2D solid on a uniform substrate; this triangular floating solid may in general be incommensurate with the periodic substrate. Increasing temperature, the floating solid is expected to melt at T_m, via the dislocation unbinding mechanism, into a liquid phase. On a triangular substrate, this liquid will have a small (but finite) long-ranged sixfold orientational order induced by the substrate, at all temperatures. There should, however, be a temperature T_i where $\varphi_6^\infty(T)$ shows a significant drop, reminiscent of the disclination unbinding transition on the smooth substrate. This drop should become increasingly sharper as the ratio of substrate period to particle separation becomes smaller. On the square substrate, Nelson and Halperin predict that there will be a sharp Ising transition at a $T_i > T_m$, where quasi-long-range sixfold orientational order in the liquid vanishes, and only the long-range fourfold orientational order induced by the substrate remains. This Ising transition can be viewed as a "ghost" of the hexatic to normal liquid transition, which would occur in the absence of the periodic substrate. The fourfold orientational order, induced by the substrate, again persists at all higher temperatures.

To conclude, we note again that the properties of the 2D floating solid, described above, follow solely from continuum elastic theory, independent any particular theory of melting. It is the existence of the hexatic liquid phase that is a specific prediction of the KTNHY melting theory. However, as pointed out by Nelson and Halperin,[20] it is always possible that a "premature" unbinding of disclination pairs may lead to a direct melting of the 2D solid into the normal liquid. Such a transition is then expected to be first order. In this case, the KTNHY prediction, Eq. (17), for the universal value of $\eta_{\mathbf{G}}^{-1}$ at melting, becomes a lower bound, $\eta_{\mathbf{G}_1}^{-1}(T_m^-) \geq 3$. Results from various numerical simulations and experiments[35] indicate that this first-order behavior might indeed be prevailing in the various 2D systems studied so far.

D. Observables and finite-size scaling

We now show how the predictions of the preceding section translate into the behavior of observables which can be directly measured in our MC simulation. There are

two key issues that we wish to investigate in the superconducting networks: (i) the transition from the superconducting to the normal state and (ii) the melting of the magnetic-field-induced vortex lattice. For (ii), our goal is to test the KTNHY theory of 2D melting, and so we will be interested in studying both the translational and the orientational order of the vortex lattice.

The superconducting to normal transition, marked by the loss of superconducting phase coherence, is measured by the vanishing of the *helicity modulus*, $\Upsilon(T)$, which measures the response of the system to applying a net twist, or phase gradient, to the phases θ_i in the Hamiltonian, Eq. (1). For the Villain interaction of Eq. (4), the helicity modulus can be shown[27] to be identical to the inverse dielectric function of the corresponding Coulomb gas of Eq. (5), $\Upsilon/J_0 = \epsilon^{-1}$, where ϵ^{-1} is defined in the usual way,

$$\epsilon^{-1}(T) = \lim_{k\to 0}\left\{1 - \frac{2\pi}{TNk^2}\langle n_{\mathbf{k}} n_{-\mathbf{k}}\rangle\right\}. \tag{20}$$

Here $n_{\mathbf{k}} = \sum_i n_i \exp(-i\mathbf{k}\cdot\mathbf{r}_i)$ is the Fourier-transformed charge density. The vanishing of ϵ^{-1} signals an insulator-to-metal transition in the Coulomb gas. The free charges characteristic of the conducting phase correspond to freely diffusing vortices in the superconducting network, which are responsible for the loss of phase coherence.[19] In the simulation, the $\mathbf{k}\to 0$ limit is approximated by averaging ϵ^{-1} over the smallest allowed nonzero wave vectors.

Information on the translational order in the vortex lattice can be extracted from the *structure function*

$$S(\mathbf{k}) = \frac{1}{N_c}\langle n_{\mathbf{k}} n_{-\mathbf{k}}\rangle \equiv \frac{1}{N_c}\sum_{ij} e^{i\mathbf{k}\cdot(\mathbf{r}_i - \mathbf{r}_j)}\langle n_i n_j\rangle, \tag{21}$$

which we evaluate for all allowed wave vectors $\mathbf{k} = (m_1/L)\mathbf{b}_1 + (m_2/L)\mathbf{b}_2$ in the first Brillouin zone (BZ) of the reciprocal lattice to the real space dual lattice of the superconducting network. A 2D intensity plot of $S(\mathbf{k})$ serves as a simple tool for visualization of the different phases in the system. In analogy to the conventional x-ray scattering images, we expect $S(\mathbf{k})$ to display a periodic array of sharp δ-function Bragg peaks in a state with long-range translational order, and a set of smooth concentric rings in a normal liquid phase. A phase with quasi-long-range translational order, characterized by algebraic translational correlations, will be distinguished by a regular array of algebraically diverging peaks of finite width.[35] A hexatic liquid phase should appear as a set of concentric rings with sixfold angular modulation.

Apart from providing the simple visualization described above, the scaling of the heights of the peaks in $S(\mathbf{k})$, as a function of system size L, will serve as a good quantitative indicator of translational correlations in the system. Combining the definition of $S(\mathbf{k})$ in Eq. (21) with Eq. (14) [note that, in Eq. (21), $n_i = 1$ on a site containing a vortex and $n_i = 0$ on a site without a vortex] one easily obtains

$$\frac{S(\mathbf{G})}{L^2} \sim \begin{cases} 1 & \text{in pinned solid } (T < T_c)\,, \quad (22a)\\ L^{-\eta_{\mathbf{G}}(T)} & \text{in floating solid } (T_c < T < T_m)\,, \quad (22b)\\ (\xi_+/L)^2 & \text{in hexatic or normal liquid } (T > T_m)\,. \quad (22c)\end{cases}$$

The finite-size scaling analysis of the translational order, which we present in Sec. III, will be based on the above relations. In particular, a comparison of Eqs. (22) with our MC data will allow us to extract the temperature-dependent exponent $\eta_{\mathbf{G}}(T)$ and test the KTNHY prediction regarding the universal jump in $\eta^{-1}_{\mathbf{G}_1}(T_m^-)$. We shall also determine the correlation length $\xi_+(T)$ in the liquid phase.

There is an independent way to extract the exponents $\eta_{\mathbf{G}}$ (and thus the vortex shear modulus μ) without having to use finite-size scaling. One can instead, for a given system size, fit to the heights of the peaks $S(\mathbf{G})$, as a function of $|\mathbf{G}|$. For the low-order peaks, this dependence is roughly Gaussian, as can be seen by combining Eq. (22b) with the expression for $\eta_{\mathbf{G}}$ in Eq. (16). For the higher-order peaks, however, we need to rederive this dependence, since the prefactor [which is not shown in Eq. (22b)] becomes important. Substituting Eq. (14) into the definition of the structure function, Eq. (21), and approximating the summations by integrations, we get

$$S(\mathbf{G}) = c\int d^2r (r/a_v)^{-\eta_{\mathbf{G}}} \simeq 2\pi c a_v^{-\eta_{\mathbf{G}}}\int_{a_v}^{R} dr r^{1-\eta_{\mathbf{G}}}, \tag{23}$$

where $R \sim L$ is a long-distance cutoff, a_v is the average separation between vortices, and c is a proportionality constant of the order 1. The integral is easily evaluated,

$$S(\mathbf{G})/L^2 \simeq \frac{2\pi c}{2-\eta_{\mathbf{G}}}\left[(R/a_v)^{-\eta_{\mathbf{G}}} - (R/a_v)^{-2}\right], \tag{24}$$

and c is determined by the requirement that $S(0)/L^2 = 1$. One can see that for $\eta_{\mathbf{G}} \ll 2$ formula (22b) remains valid, but for $\eta_{\mathbf{G}} \simeq 2$ it breaks down. In practice, since $\eta_{\mathbf{G}_1} < 1/3$ by the KTNHY bound, and any exponent $\eta_{\mathbf{G}}$ at a given fixed temperature can be written as

$$\eta_{\mathbf{G}} = \eta_{\mathbf{G}_1}(|\mathbf{G}|^2/|\mathbf{G}_1|^2), \tag{25}$$

formula (22b) will approximately hold for the three shortest reciprocal lattice vectors $\mathbf{G}$ only. To draw quantitative conclusions regarding the exponent $\eta_{\mathbf{G}}$, one must use the more accurate relation of Eq. (24).

Information on the bond orientational order will be obtained by measuring the fourfold and sixfold *orientational correlation*

$$\varphi_p(T) = \frac{1}{N_c^2}\sum_{ij}\langle e^{ip(\vartheta_i - \vartheta_j)}\rangle,\ p = 4, 6\,, \tag{26}$$

where the sum is over sites with nonvanishing charges $n_i = +1$, and ϑ_i is the bond orientation angle defined in the previous section. For a finite system, one expects to see a sharp drop in $\varphi_p(T)$ at the transition from an orientationally ordered phase, to a disordered or possibly hexatic phase. One can deduce the scaling of the orientational correlation $\varphi_6(T)$ with system size L, by combining Eq. (26) with the KTNHY prediction of Eq. (18),

$$\varphi_6 \sim \begin{cases} 2\pi\alpha(\xi_6'/L)^2 + \varphi_6^{\infty} & \text{in pinned or floating solid } (0 < T < T_m), \quad (27a) \\ L^{-\eta_6(T)} & \text{in hexatic liquid } (T_m < T < T_i), \quad (27b) \\ (\xi_6/L)^2 & \text{in normal liquid } (T > T_i). \quad (27c) \end{cases}$$

Relations (27aa) and (27ac) hold for $L \gg \xi_6$ [otherwise one must include corrections $\sim \exp(-L/\xi_6)$]. These scaling relations for φ_6 will be used extensively in our analysis, to test for the existence of a hexatic phase in our model.

E. Monte Carlo algorithm

For the purpose of developing a fast MC algorithm, it is important to realize that the physical phenomena described in the previous section occur at temperatures which are about one order of magnitude lower[32] than the ordinary Kosterlitz-Thouless transition[30] in the zero magnetic field, $f = 0$, case. This implies that the role of vortex-antivortex pair excitations is negligible in the temperature range that we study, and that in the simulation we can restrict ourselves to the excitations caused by movement of the vortices induced by the external magnetic field $\mathbf{B}$. We have explicitly verified that the energy of an isolated vortex-antivortex pair [in the Coulomb gas language a pair of $(+,-)$ charges] is always $E_{\text{pair}} \gg k_B T$, and thus in practice such an excitation would never be accepted in the MC simulation. Consequently, our updating scheme is as follows. In each step, one charge is selected at random and moved to a different site within a radius r_0, which is chosen so as to maximize the acceptance rate. We find that values $r_0 \sim a_v/2$ are optimal. The energy change $\Delta E = E_{\text{new}} - E_{\text{old}}$ is then computed, and the excitation is accepted or rejected according to the standard Metropolis algorithm:

$$\text{accept if } e^{-\Delta E/T} > x,$$

where x is a random number uniformly distributed on the interval $[0,1)$. Here and henceforth, we work in units in which $k_B \equiv 1$. N_c such attempts we will refer to as one MC sweep. At low temperature, we also made global moves, by attempting to shift entire rows of charges by one space. Such moves are meant to model long-wavelength shear excitations, and help to accelerate equilibration near the vortex-lattice melting transition.

Due to the long-ranged nature of the Coulomb potential, the most time-consuming operation is the evaluation of ΔE. From Eq. (5) we find that the energy change for moving a charge from the site $\mathbf{R}_1$ to the site $\mathbf{R}_2$ is

$$\Delta E = -\sum_j V'(\mathbf{R}_1 - \mathbf{r}_j)n_j + \sum_j V'(\mathbf{R}_2 - \mathbf{r}_j)n_j - V'(\mathbf{R}_1 - \mathbf{R}_2), \quad (28)$$

where we have used the fact that $V'(-\mathbf{r}) = V'(\mathbf{r})$ and $V'(0) = 0$. In this form, each evaluation of ΔE is a computation of the order N_c, as j sweeps through all the sites with nonvanishing charge $n_j = +1$. To speed up this process, we use an algorithm developed by Grest.[36] At each site of the lattice we define a potential due to all charges in the system,

$$F(\mathbf{r}_i) = \sum_j V'(\mathbf{r}_i - \mathbf{r}_j)n_j. \quad (29)$$

Now each evaluation of

$$\Delta E = -F(\mathbf{R}_1) + F(\mathbf{R}_2) - V'(\mathbf{R}_1 - \mathbf{R}_2) \quad (30)$$

requires computation of only $O(1)$. Naturally, each time the excitation is accepted, it is necessary to update $F(\mathbf{r}_i)$ at all sites,

$$F_{\text{new}}(\mathbf{r}_i) = F_{\text{old}}(\mathbf{r}_i) - V'(\mathbf{r}_i - \mathbf{R}_1) + V'(\mathbf{r}_i - \mathbf{R}_2), \quad i = 1, 2, \ldots, N. \quad (31)$$

This is a computation of order N. However, since the acceptance rate in the interesting temperature range is very low (typically below 1%), this method is faster than the direct approach of Eq. (28).

Data are collected by heating the system up from the ground state. At each temperature we discard 30 000 MC sweeps to equilibrate the system. Then, starting from this equilibrated configuration, we perform several (typically 4–6) independent runs of 100 000 sweeps each to sample physical quantities. In some cases, when evaluating quantities at the temperatures close to the critical point, substantially longer runs are carried out. Errors are estimated from the standard deviation of these independent runs. To verify the consistency of our results, we also perform cooling from a random configuration at high temperature; no substantial hysteresis is found.

All simulations were carried out on Sparc 10 workstations. The time needed to equilibrate the system and sample the physical quantities at a given temperature T was typically several hours (depending on size) using 100% of the single processor power. For example, it took approximately 3 h to carry out 100 000 MC sweeps at a temperature close to melting, for a medium-sized system $N_c = 81$ with density $f = 1/49$. Our longest run, to sample the energy distribution near the depinning transition, took 189 h for 4×10^7 MC sweeps on the largest system of $N_c = 169$ and $f = 1/49$.

III. SIMULATIONS ON THE TRIANGULAR GRID: DILUTE CASE

A. Results

In this section we report our results from simulations of the Coulomb gas Hamiltonian (5) on a triangular grid of sites (corresponding to a honeycomb superconducting network), for the dilute limit $f \ll 1$ (or equivalently $a_0 \ll a_v$). In this case, we expect that our discretized model will well approximate the continuum. Some of these results have been reported by us previously.[37] The advantage of choosing a triangular grid is that, for a given system size L, one can always choose f in such a way so as to accommodate a perfect, commensurate, triangular vortex lattice in the ground state. By contrast, this is never possible on a square grid. It is convenient to choose $f = 1/m^2$, with m integer, since then each system size of the form $L = sm$ (s integer) will accommodate a triangular ground state with $N_c \equiv fL^2 = s^2$ vortices. We have studied systematically densities $f = 1/m^2$, with m=3–12, and fixed $N_c \simeq 100$. The results of our investigation are summarized in Fig. 1: For sufficiently dilute systems ($f < 1/25$) we find three distinct phases. At low temperatures the vortex lattice is in a "pinned solid" phase, locked to the underlying grid. Above a sharp depinning temperature $T_c(f)$, the vortices are in a "floating solid" phase, which then melts at T_m into a normal vortex liquid. The properties of these phases will be discussed below. For denser systems with $f > 1/25$, the two transitions at T_c and T_m merge, and there is only a single transition from a pinned solid into a liquid.

For a simple visualization of the three phases, we show in Fig. 2 intensity plots of $S(\mathbf{k})$ at various T, for the specific case of $f = 1/49$ and $N_c = 63$. We also display the amplitude of $S(\mathbf{k})$ along the symmetry axis k_y. For $T = 0.003$ [Fig. 2(a)], just below $T_c(f)$, we see a regular array of δ-function Bragg peaks, indicating long-ranged translational order induced by pinning to the triangular grid. The width of these peaks corresponds to the finite resolution of wave vectors allowed by our finite system. At $T = 0.0065$ [Fig. 2(b)], just below T_m, we see a regular array of peaks, but they are now of finite width. We will show that these peaks are consistent with the power-law singularities characteristic of the algebraic translational correlations expected for a 2D floating solid phase. The heights of the peaks along the symmetry axis are well described by a Gaussian, as expected from Eqs. (24) and (25). Thus, for $T_c(f) < T < T_m$ we do have a floating vortex lattice, as in the continuum limit. For $T = 0.0075$ [Fig. 2(c)], slightly above T_m we see a rotationally invariant structure, typical for a liquid with short-range correlations. Thus, for $T > T_m$, the floating vortex lattice has melted into a normal liquid. It is interesting to note that we see no sign of angular modulation in the rings above T_m. One might expect such a modulation due to the long-ranged sixfold orientational order induced in principle by the underlying triangular grid; if the grid was too fine for this effect to be significant, modulation might still be present if a hexatic phase existed just above T_m.

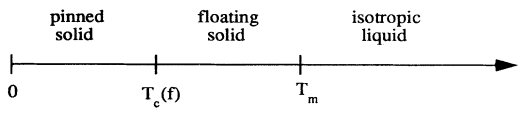

FIG. 1. Phase diagram of the sufficiently dilute system, as found by our Monte Carlo calculation.

In Fig. 3, we plot versus T the inverse dielectric function $\epsilon^{-1}(T)$, and the orientation order correlation $\varphi_6(T)$, for $f = 1/49$ and $N_c = 169$ (one of the largest systems that we have studied). We see that $\epsilon^{-1}(T)$ vanishes at the depinning transition $T_c(f)$, signaling the loss of superconducting phase coherence in the floating solid phase. This is just a reflection of the fact that an unpinned vortex lattice, in the presence of any applied dc current (no matter how small), will be free to drift transversely to the current, resulting in a finite linear "flux flow" resistance. Our results explicitly show that the absence of phase coherence in this $\mathbf{k} \to 0$ sense does not imply the absence of a well-defined vortex lattice. Considering the orientation order, we see that φ_6 sharply drops at $T_c(f)$, but remains finite up to the melting temperature T_m, where it drops again sharply to nearly zero values. The smallness of φ_6 above T_m indicates that the sixfold orientational long-range order, which is induced in principle by the triangular grid, is indeed a negligibly small effect at the densities we are concerned with. We shall discuss this point in more detail in the following section. In Fig. 4, we show the dependence of $T_c(f)$ and T_m on the vortex density f, as estimated from the behavior of $\epsilon^{-1}(T)$ and $\varphi_6(T)$, and checked against the behavior of the structure function $S(\mathbf{k})$. We see that only for sufficiently dilute systems, $f < 1/25$, is there a floating solid phase; for $f > 1/25$ there is only a single transition from a pinned solid to a liquid. As f decreases, $T_c(f)$ vanishes linearly with f, consistent with the TJ conjecture[5] for the loss of superconducting coherence. T_m, however, quickly approaches a finite constant $T_m = 0.0070 \pm 0.0005$. In terms of the superconductor temperature, this means a vortex lattice melting at $T_m = 0.0070\Phi_0^2/8\pi^2\lambda_\perp$. This is well within the bounds $0.0046 < T_m < 0.0086$ estimated by Fisher[32] from the KTNHY theory.

B. Melting transition: finite-size scaling analysis

To investigate if the melting transition at T_m is indeed consistent with the KTNHY theory, we have carried out a detailed finite-size scaling analysis for the density $f = 1/49$. This density has been chosen for two reasons. First, the estimated T_m is well separated from the depinning temperature T_c, and hence the floating solid phase exists in a relatively wide interval of temperatures. Second, the density is not too small, and thus we are able to study systems with as many as $N_c = 169$ vortices. More dilute systems, with comparable N_c would require sizes that are currently out of reach of the computer power available to us. We have carried out extensive simulations for the system sizes $L = 28, 35, \ldots, 91$, and we have analyzed the size dependences of various physical quan-

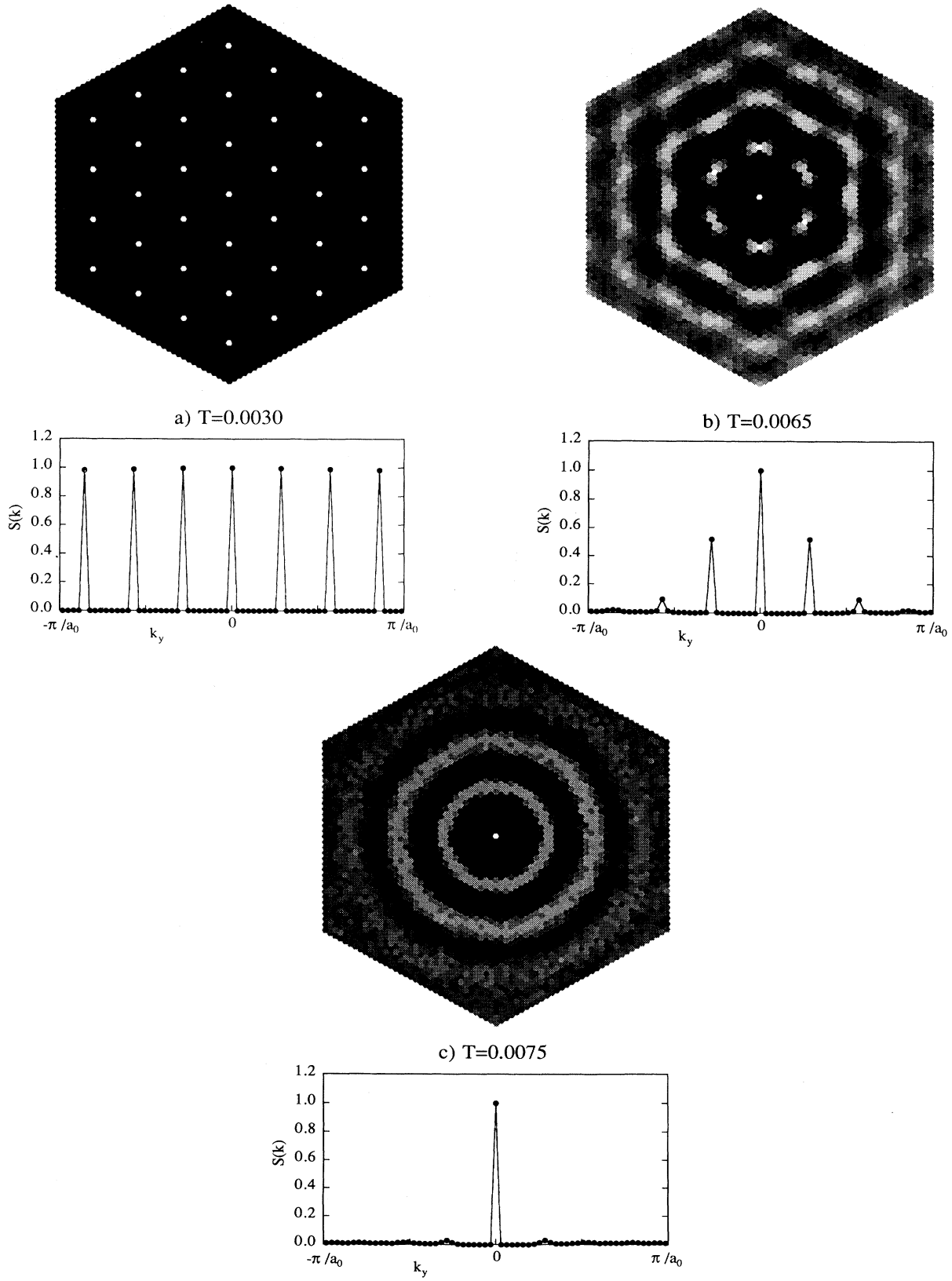

FIG. 2. Structure function $S(\mathbf{k})$ in the first Brillouin zone (upper portion of the figure) and the profile of the peak heights along the vertical symmetry axis k_y (lower portion), for $f = 1/49$ and $N_c = 63$, and three different temperatures T: (a) $T = 0.003$, just below T_c, in the "pinned solid" phase, (b) $T = 0.0065$, just below T_m, in the "floating solid" phase, (c) $T = 0.0075$, just above T_m, in the liquid. Intensities in the density plots are plotted nonlinearly to enhance features.

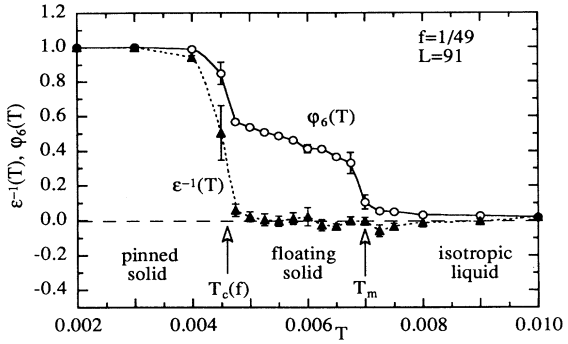

FIG. 3. Inverse dielectric function $\epsilon^{-1}(T)$ and orientational order correlation $\varphi_6(T)$ versus T for $f = 1/49$ and $N_c = 169$. Solid and dashed lines are guides to the eye only.

tities at several temperatures below and above T_m. Our results are as follows.

In Fig. 5 we plot $S(\mathbf{G}_1)/L^2$ as a function of L, on a log-log scale, for several different temperatures. Data for each temperature fall on a straight line, confirming the expected power-law behavior of Eq. (22). These straight lines fall into three distinct groups. For $T < T_c \simeq 0.0045$, $S(\mathbf{G}_1)/L^2 \sim 1$, indicating the long-range order of the pinned lattice. For $T_c < T < T_m \simeq 0.007$, we find algebraic decay, $S(\mathbf{G}_1)/L^2 \sim L^{-\eta_{\mathbf{G}}(T)}$. For $T > T_m$, we find $S(\mathbf{G}_1)/L^2 \sim L^{-x}$, with $x \to 2$ as T increases, consistent with the short-range order of a liquid.

Thus, our data for the floating solid phase are consistent with the predictions of the continuum elastic theory, given by Eq. (22b), and in particular we may fit our data to this expression to obtain the translational correlation exponent $\eta_{\mathbf{G}_1}$. We show our results in Table I. We can now make quantitative comparison with the KTNHY theory, by noting that $\eta_{\mathbf{G}_1}$ first exceeds the KTNHY universal value of 1/3 [see Eq. (17)] at $T = 0.0065$, very close to the melting temperature $T_m \simeq 0.0070$ as estimated from the behavior of the orientational correlation $\varphi_6(T)$ of Fig. 3. The slopes of the lines in Fig. 5 also show an apparent discontinuous jump at this same T_m.

As a consistency check, we have also computed $\eta_{\mathbf{G}_2}$,

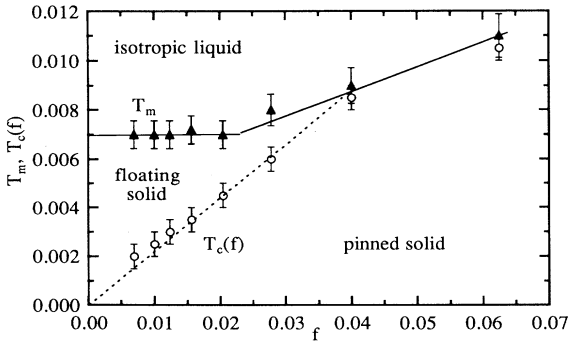

FIG. 4. The dependence of the depinning and melting temperatures, T_c and T_m, on vortex density f. Errors are estimated from the width in the apparent drop in $\epsilon^{-1}(T)$ and $\varphi_6(T)$. Solid and dashed lines are guides to the eye only.

where $\mathbf{G}_2 = 2\mathbf{G}_1$. Using similar fits to $S(\mathbf{G}_2)$ as in Fig. 5, we determine the exponent $\eta_{\mathbf{G}_2}$, and show the results in Table I. We see that $\eta_{\mathbf{G}_2} \simeq 4\eta_{\mathbf{G}_1}$ as expected, since, according to Eq. (19), $\eta_{\mathbf{G}} \sim |\mathbf{G}|^2$.

As an alternative way of calculating $\eta_{\mathbf{G}_1}$, we fit to the heights of the peaks in $S(\mathbf{k})$ at all the available $\mathbf{G}$, for a fixed size system, as described in Eqs. (23)–(25). We found that the results are only weakly dependent on the precise value of the cutoff R of Eq. (24); we therefore take $R = L$, which results in an excellent fit. We show one example of such a fit in Fig. 6. The exponent $\eta_{\mathbf{G}_1}(T)$, obtained in this way, is shown in Table II for the sizes $L = 63, 77, 91$, with $f = 1/49$. We note that despite a certain tendency to overestimation, these exponents are in reasonable agreement with those obtained from the finite-size scaling. This method of extracting the shear modulus should be useful in situations where a finite-size scaling analysis is difficult to handle, such as in systems with a large unit cell in the ground state.

Let us now consider the orientational order. In Fig. 7 we plot the orientational correlation $\varphi_6(T)$ as a function of L for several temperatures. In the pinned solid, $T < T_c$, $\varphi_6(T) \to 1$ as L increases, confirming the expected long-ranged orientational order of the perfect pinned triangular lattice. More interestingly, $\varphi_6(T)$ also approaches a finite value φ_6^∞ in the floating lattice phase, $T_c < T < T_m$, in agreement with continuum elastic theory. The solid lines in Fig. 7 are from least squares fits to Eq. (27a). The resulting fitted values of φ_6^∞ are shown in Table I. Above T_m we attempt to fit to the power law of Eq. (27b) for a hexatic liquid, but we always find that using Eq. (27c) for an isotropic liquid results in a distinctly better fit. Since the underlying triangular grid will in principle result in long-range sixfold order at all temperatures, we have also fit our data above T_m to the form of Eq. (27a), which differs from Eq. (27c) only in the constant φ_6^∞. As shown in Table I, however, we always find $\varphi_6^\infty \simeq 0$. Thus the discrete grid is playing a negligible role in the orientation order. To compare our fits above T_m, we note that in most cases the χ^2 parameter of the fit to Eq. (27a) is 5–10 times smaller than that of Eq. (27b). The former fit is also much more stable in the sense that fitted parameters do not change significantly when the data are restricted to different ranges of L. We may therefore conclude that, in agreement with our investigation of the structure function, the floating solid melts directly into a normal liquid. The hexatic phase is either absent in our system, or it occurs only in some extremely narrow interval of temperatures, which makes it difficult to detect by numerical simulation.

In order to see this another way, in Fig. 8 we plot versus temperature our values of $\varphi_6^\infty(T)$ and $T/\eta_{\mathbf{G}_1}(T)$, obtained from our finite-size scaling analysis. From Eq. (16) we see that $T/\eta_{\mathbf{G}_1}(T)$ is just proportional to the vortex lattice shear modulus μ. We see that $\varphi_6^\infty(T)$ starts to drop at the same temperature that $T/\eta_{\mathbf{G}_1}(T)$ first drops below the KTNHY universal value of $3T$ [see Eq. (17)], i.e., the temperature at which the floating solid starts to melt. The temperature range over which φ_6^∞ decays to zero is identical to the range over which $T/\eta_{\mathbf{G}_1}(T)$ decays. This suggests that the small but finite values of

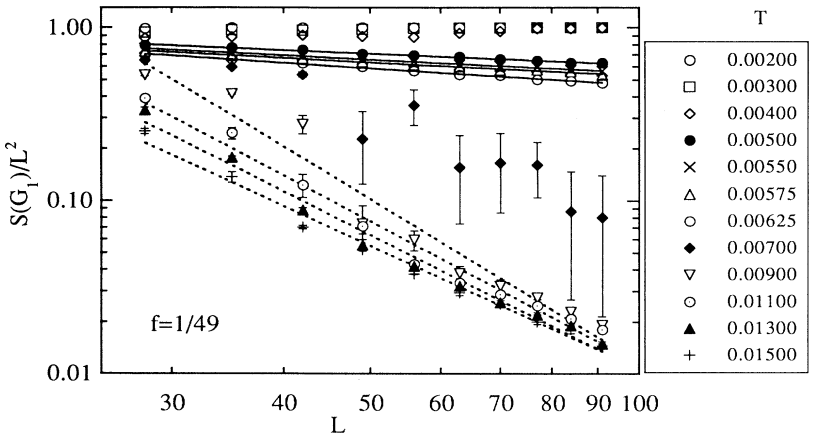

FIG. 5. Finite-size scaling of $S(\mathbf{G}_1)/L^2$ (note the log-log scale) for $f = 1/49$. Solid and dashed lines are fits to Eq. (22b).

φ_6^∞ which we find above T_m are just a finite-size effect, rather than a signature of the hexatic phase. Let us also note that the exponent $\eta_{\mathbf{G}_1}(T)$ has a physical meaning only below T_m. Above T_m it is strictly infinite and we use it here, with some abuse of notation, simply as the exponent resulting from the fit of our data to the power-law form of Eq. (22b).

Having obtained the values of $\eta_{\mathbf{G}_1}(T)$ and $\varphi_6^\infty(T)$, we can now test the relation, Eq. (19), between the orientational long-range order and the vortex-lattice shear modulus μ that should hold in the floating solid phase. Expressing μ in terms of the exponent $\eta_{\mathbf{G}_1}$, Eq. (19) gives

$$\eta_{\mathbf{G}}(T) = -K \ln[\varphi_6^\infty(T)], \tag{32}$$

with $K = 2|\mathbf{G}|^2/9\Lambda^2$, where $\Lambda = \lambda(2\pi/a_v)$, and λ is a dimensionless constant of order unity. In Fig. 9 we plot $\eta_{\mathbf{G}_1}^{-1}(T)$ and $-1/K \ln[\varphi_6^\infty(T)]$ versus temperature. For $K = 0.33$, which corresponds to $\lambda = 0.94$, the two data sets lie on top of each other for all T below T_m, providing yet another consistency check for our calculation.

By fitting our data above T_m to Eqs. (22c) and (27c) we have also extracted the correlation lengths $\xi_+(T)$, associated with translational order, and $\xi_6(T)$, associated with sixfold bond orientational order. We are able to determine these from finite-size scaling only up to an overall multiplicative factor. We determine this factor by assuming that at high T the correlation lengths are equal to the average spacing between vortices, i.e., $\xi(T \to \infty) = a_v$. With this assumption, $\xi_+(T)$ and $\xi_6(T)$ are displayed in Fig. 10. We see that both correlation lengths rapidly increase around $T \simeq 0.007$. It is also evident from Fig. 10 that orientational correlations persist out to longer distances, up to higher temperatures, than translational correlations.

TABLE I. Temperature dependence of the exponents $\eta_{\mathbf{G}_1}(T)$ and $\eta_{\mathbf{G}_2}(T)$ for $f = 1/49$ on the triangular grid, as obtained from finite-size scaling. Also displayed are the limiting values φ_6^∞ of the orientational correlation $\varphi_6(T)$ for $L \to \infty$.

T	$\eta_{\mathbf{G}_1}(T)$	$\eta_{\mathbf{G}_2}(T)$	φ_6^∞
0.00475	0.188 ±0.008	0.704 ±0.055	0.571 ±0.007
0.00500	0.207 ±0.007	0.806 ±0.032	0.529 ±0.005
0.00525	0.211 ±0.007	0.852 ±0.028	0.504 ±0.004
0.00550	0.248 ±0.005	0.998 ±0.019	0.476 ±0.003
0.00575	0.255 ±0.008	0.999 ±0.029	0.458 ±0.003
0.00600	0.296 ±0.006	1.065 ±0.028	0.426 ±0.007
0.00625	0.319 ±0.010	1.191 ±0.016	0.403 ±0.004
0.00650	0.4 ±0.16	1.4 ±0.22	0.33 ±0.030
0.00675	1.4 ±0.31	2.0 ±0.31	0.20 ±0.041
0.00750	3.4 ±0.37	3.4 ±0.44	0.03 ±0.046
0.01100	2.8 ±0.23	2.9 ±0.30	-0.01 ±0.032
0.01500	2.2 ±0.12	2.1 ±0.22	0.00 ±0.020

C. Order of the melting transition

The absence of the hexatic phase, as deduced from our analysis of the orientational correlations, suggests the possibility that the transition is not of the KTNHY type, but is due to some other mechanism, such as domain wall proliferation. It might also be that the unbinding of disclinations occurs simultaneously with the unbinding of dislocations. Such a possibility has been suggested in Ref. 20. In any case, it is useful to determine the order of this melting transition. To examine the possibility that the transition is first order, we have used the histogram method due to Lee and Kosterlitz.[38] For various system

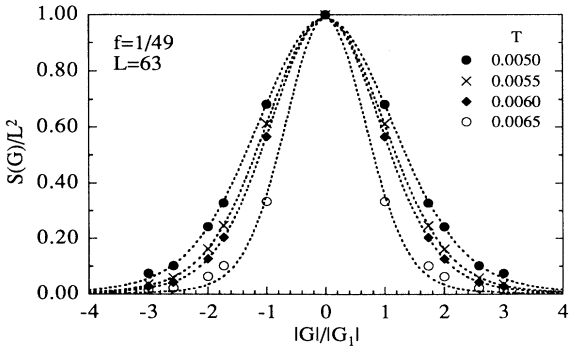

FIG. 6. Heights of the peaks $S(\mathbf{G})$ versus $|\mathbf{G}|$ for $f = 1/49$ and $L = 63$. Dashed lines represent the best fit to Eq. (24), and are used to extract the exponent $\eta_{\mathbf{G}_1}(T)$.

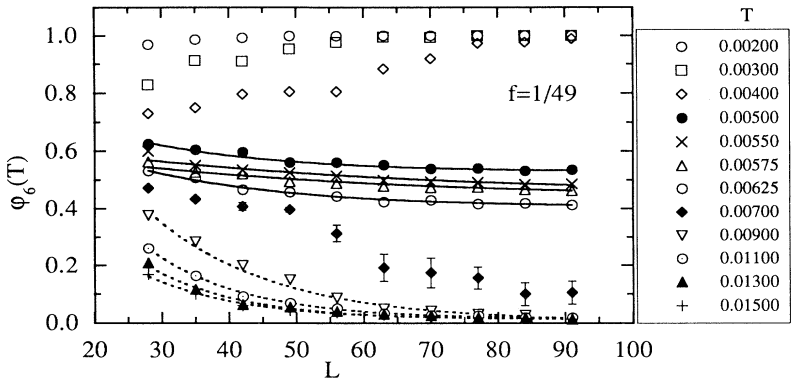

FIG. 7. Finite-size scaling of $\varphi_6(T)$ for $f = 1/49$. Solid and dashed lines are fits to Eq. (27a).

sizes at $f = 1/49$, we measure the energy distribution $P(E) \sim e^{-F(E)/T}$ near the melting temperature T_m. In Fig. 11 we plot the resulting free energy $F(E)$ versus E. Although our data are somewhat noisy, we see a clear double-well structure with an energy barrier ΔF between two coexisting phases. The inset to Fig. 11 shows the dependence of ΔF on the system size L. The energy barrier ΔF grows with L, strongly suggesting a first-order transition. Our system sizes remain too small to see clearly the predicted scaling $\Delta F \sim L$.

For all sizes, the data have been taken at $T = 0.0065$, and then the energy distribution is extrapolated, using the method of Ferrenberg and Swendsen,[39] to that temperature which gives two minima of equal depth. This criterion gives an improved estimate of the melting temperature, $T_m = 0.0066$. A total of 10^7 MC sweeps were performed for each size to measure the energy distribution $P(E)$. We have checked the consistency of these measurements by calculating the energy of the system at various temperatures (above and below T_m) using the extrapolated distributions $P(E,T)$. We then compared these with energies obtained by direct simulation at those temperatures, and found good agreement for all temperatures not too far from T_m.

To conclude, the histogram method provides strong evidence that the melting transition is first order. This is consistent with our observation that the 2D solid melts directly into an isotropic liquid. The transition is weakly first order, however, as can be seen from our result that the jump in $\eta_{\mathbf{G}_1}(T_m^-)$ (and hence the vortex lattice shear modulus μ) at melting remains very close to the KTNHY universal value.

TABLE II. Comparison of the exponents $\eta_{\mathbf{G}_1}(T)$ obtained using two different methods. Columns 2–4 show results from fitting of $S(\mathbf{G})$ to Eq. (24), for system sizes $L = 63$, 77, 91. Column 5, labeled FSS, restates the results from the finite-size scaling analysis. All exponents are for density $f = 1/49$.

T	$\eta_{\mathbf{G}_1}(T)$			
	$L = 63$	$L = 77$	$L = 91$	FSS
0.00475	0.164±0.026	0.161±0.025	0.195±0.018	0.188 ±0.008
0.00500	0.216±0.012	0.221±0.009	0.219±0.007	0.207 ±0.007
0.00525	0.249±0.009	0.235±0.009	0.247±0.006	0.211 ±0.007
0.00550	0.282±0.007	0.272±0.006	0.275±0.007	0.248 ±0.005
0.00575	0.298±0.008	0.292±0.009	0.290±0.006	0.255 ±0.008
0.00600	0.326±0.008	0.326±0.007	0.329±0.007	0.296 ±0.006
0.00625	0.351±0.014	0.350±0.017	0.352±0.016	0.319 ±0.010
0.00650	0.677±0.342	0.473±0.223	0.568±0.131	0.4±0.16
0.00675	1.755±0.789	1.678±0.453	2.458±0.911	1.4±0.31

D. Depinning transition

Finally, we consider the order of the depinning transition at $T_c(f)$. In their work on 2D melting on a periodic substrate, Nelson and Halperin[20] studied this "commensurate to floating" transition using renormalization group techniques. They concluded that the transition is most likely second order, with properties very similar to the floating solid to liquid melting transition discussed in Sec. II C. To test this prediction, we use the histogram method applied at the depinning transition $T_c(f)$, just as we did in the preceding section for melting at T_m. Measuring the energy distribution $P(E)$ at $T_c(f)$, for $f = 1/49$ and various L, we show the free energy $F(E)$ versus E in Fig. 12. As was seen at T_m, we now similarly see a pronounced double-well structure with barrier ΔF growing with the size of the system (see the inset). Again, this is a clear indication that the transition is first order. Due to the low acceptance rates at these low temperatures, we had to perform as many as 4×10^7 MC

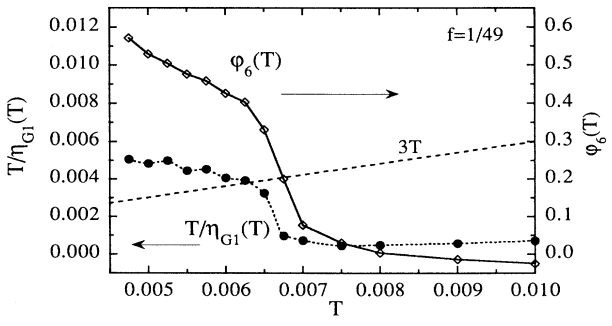

FIG. 8. $T/\eta_{\mathbf{G}_1}(T)$ (proportional to the shear modulus μ) and orientational correlation φ_6^∞ versus T, as extracted from finite-size scaling. The intersection of $T/\eta_{\mathbf{G}_1}(T)$ with the dashed line $3T$ determines the KTNHY upper bound on the melting transition $T/\eta_{\mathbf{G}_1}(T) > 3T$.

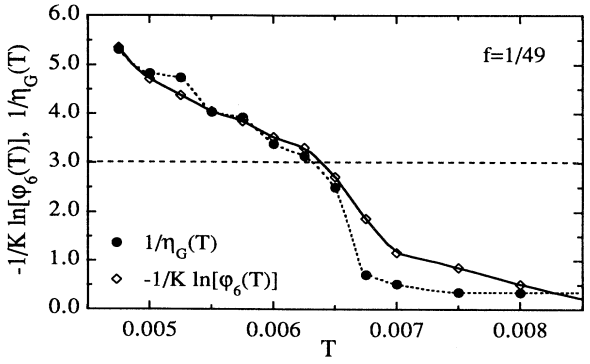

FIG. 9. Comparison of $\eta_{\mathbf{G}_1}^{-1}(T)$ and $-1/K \ln[\varphi_6^{\infty}(T)]$ as a test of Eq. (19). Below T_m the two quantities coincide, as expected for a 2D harmonic lattice. Dashed line determines the KTNHY upper bound $\eta_{\mathbf{G}_1}^{-1}(T) > 3$.

sweeps for each system size, in order to get reasonably accurate energy distributions. By finding the temperature that produces minima of equal depth, we estimate that $T_c(f = 1/49) = 0.0046$.

IV. SIMULATIONS ON THE SQUARE GRID: DILUTE CASE

A. Ground state

In the present section we shall investigate the dilute limit ($f \ll 1$) of the Coulomb gas, on a square grid of sites. This corresponds to a square periodic superconducting network, which has been the predominant geometry in experimental and theoretical studies of networks.[1,5–7] Qualitatively, we find similar behavior as found in Sec. III for the triangular grid: a depinning transition $T_c(f)$, from a commensurate pinned solid to a floating solid, followed at higher temperature by a melting transition T_m to a liquid.

While the case of a square grid is more relevant to the physics of superconducting arrays, it is somewhat more

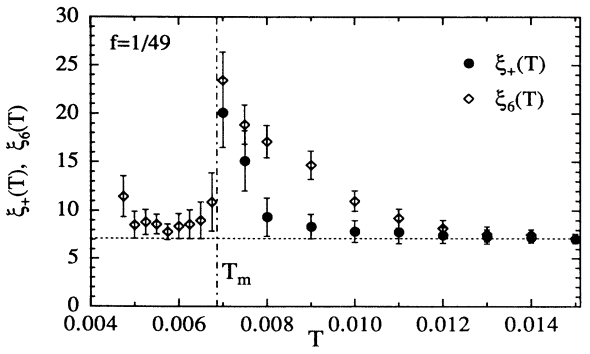

FIG. 10. Translational and orientational correlation lengths $\xi_+(T)$ and $\xi_6(T)$ versus T for $f = 1/49$, as extracted from finite-size scaling. Both correlation lengths sharply increase at the melting temperature $T_m \simeq 0.0070$.

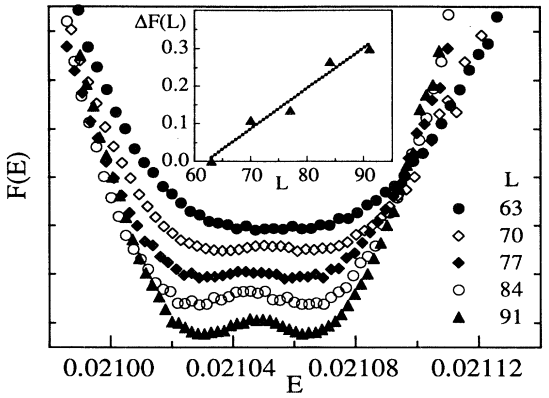

FIG. 11. Free energy distribution $F(E)$ versus E, at melting T_m, for $f = 1/49$ and several system sizes L. The growth in the energy barrier ΔF with increasing L (see inset) indicates a first-order transition. Curves for different L are offset from each other by a constant, for the sake of clarity.

difficult to study theoretically than the triangular grid of Sec. III. The main reason for this is the rich variety of ground state configurations that one can encounter for various system sizes and vortex densities f. The most extensive enumeration of such ground states, for both dilute and dense f, has been carried out by Straley and Barnett.[7] This richness in ground state structure is due to the intrinsic competition between the repulsive vortex-vortex interaction, which prefers the formation of a perfect triangular lattice, and the geometrical constraints implied by the presence of the square grid. Since a triangular lattice is incommensurate with a square grid, for small f the resulting ground states form high-order commensurate approximations to a triangular lattice that vary substantially as f varies. Thus, while in the triangular grid a density $f = 1/m^2$ can always

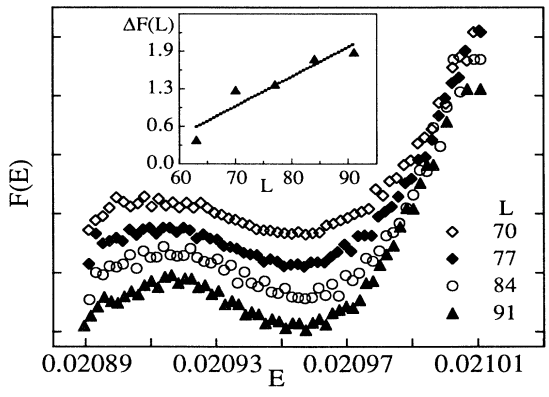

FIG. 12. Free energy distribution $F(E)$ versus E, at the depinning transition T_c, for $f = 1/49$ and several system sizes L. The growth in energy barrier ΔF with increasing L (see inset) indicates a first-order transition. Curves for different L are offset from each other by a constant, for the sake of clarity. The abrupt ending of the distributions at the low-energy side of the graph is because the lower minimum represents the ground state energy.

fit commensurably in a lattice of size $L = sm$ (s integer), for the square grid, a density of $f = 1/q$ (q integer) will require a lattice of at least $L = sq$ to contain the commensurate ground state. It thus becomes too difficult to carry out detailed finite-size scaling calculations at small f, as the lattice sizes needed quickly become too large to simulate. We therefore must be content with a more qualitative analysis based on simulations at a fixed size system. A second problem, related to the high-order commensurability of the ground state, is the existence of excited states that are nearly degenerate in energy with the ground state. This can sometimes cause equilibration problems, or leave uncertainty as to the configuration of the true ground state. Fortunately, these difficulties occur only at low temperatures, below the depinning transition $T_c(f)$, where commensurability effects are crucial. In sufficiently dilute systems, the melting of the floating solid phase at T_m is largely unaffected by such difficulties, and we find results familiar to the preceding section.

We have performed simulations for systems with a wide spectrum of densities $f = 1/q$ (q integer) with $10 < q < 90$. From inspection of the inverse dielectric constant $\epsilon^{-1}(T)$ and the orientational correlation $\varphi_6(T)$, for a fixed size L, we estimate the depinning and melting transition temperatures, $T_c(f)$ and T_m, and we plot these values versus f in Fig. 13. We see that above $f \simeq 1/30$ the depinning and melting transitions merge, and there is only a single transition from pinned solid to liquid. Due to the varying commensurability of the ground state as f varies, the values $T_c(f)$ and T_m no longer decrease monotonically with f, as was found for the triangular grid. Nevertheless, we see that $T_c(f)$ still tends linearly to zero as f decreases (dashed line), in agreement with the TJ conjecture. T_m appears to saturate around 0.007, in agreement with the melting temperature found for the triangular grid.

In order to find the ground state of the system for a given density f and size L, we have devised a simple program that scans all possible periodic vortex configurations, consistent with periodic boundary conditions, and evaluates their energy. When translational and inversion symmetries are accounted for, the total number of distinct configurations is relatively small, and even for the largest of the systems that we considered it took only few minutes to execute the program. The lowest-energy configuration obtained in this manner was then taken as a candidate for the ground state. In many cases we have verified that this indeed was a true ground state by performing a slow MC cooling from a random configuration at high temperature. In all cases we found that for $f = 1/q$ the ground state has a $q \times q$ periodicity. In Fig. 14 we display two typical examples of these ground state configurations. The almost perfect triangular lattice ($\sqrt{68} \times \sqrt{68} \times \sqrt{72}$) in Fig. 14(a) is for $f = 1/60$. Figure 14(b) shows the example of a nearly square vortex lattice ($\sqrt{50} \times \sqrt{53} \times \sqrt{89}$) with $f = 1/51$. In what follows we shall concentrate on these two special cases as representatives of two classes of systems with slightly different physical properties.

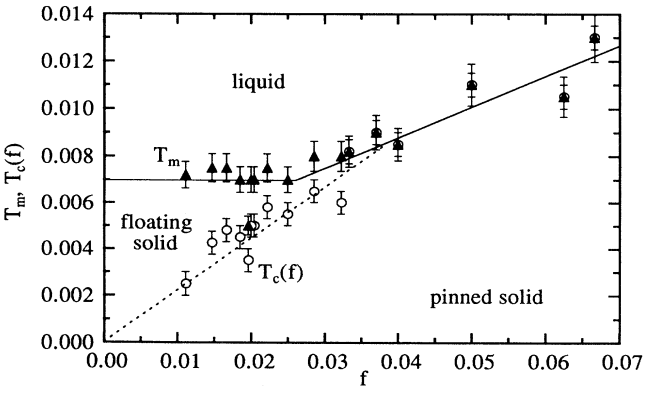

FIG. 13. Dependence of T_c and T_m on vortex density f for the dilute system on a square grid. Dashed and solid lines are guides to the eye only.

B. Systems with "nearly triangular" ground state: $f = 1/60$

Not very surprisingly, systems with an almost triangular ground state, such as $f = 1/60$ shown in Fig. 14(a),

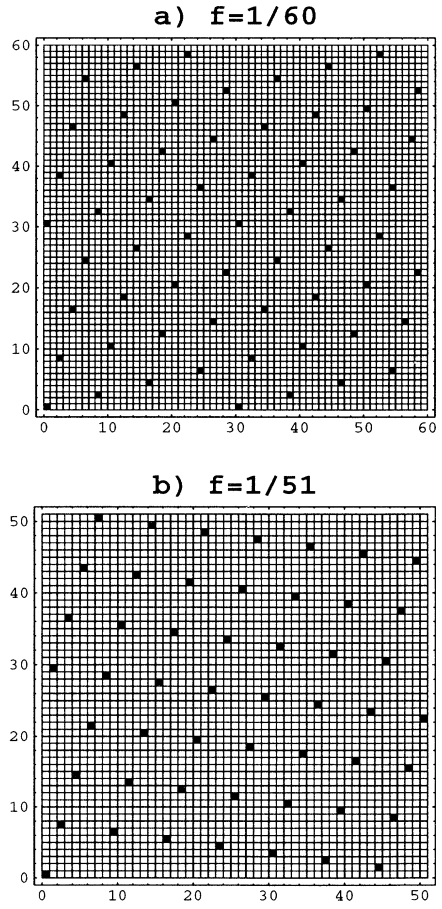

FIG. 14. Two types of ground state configurations for a dilute system on the square grid: (a) nearly triangular vortex lattice $f = 1/60$, (b) nearly square vortex lattice $f = 1/51$. Solid squares denote positions of vortices.

behave in a fashion similar to systems on the triangular grid studied in Sec. III. We display the behavior of the inverse dielectric function $\epsilon^{-1}(T)$ for $f = 1/60$ and $L = 60$ in Fig. 15(a). In Fig. 15(b) we show the sixfold and fourfold orientational correlations $\varphi_6(T)$ and $\varphi_4(T)$. A sharp drop in $\epsilon^{-1}(T)$ around $T_c(f) \simeq 0.0045$ signals the loss of superconducting phase coherence. Above $T_c(f)$, ϵ^{-1} is zero, but $\varphi_6(T)$ stays finite. Based on our experience from the triangular grid, we take this as a signature of a floating triangular solid with long-range orientational order. $T_c(f)$ is thus a transition from a commensurate pinned solid, to an incommensurate floating solid. Around $T_m \simeq 0.0075$ we see that $\varphi_6(T)$ drops again to very small values; we take this as a signal that the floating solid has melted into a vortex liquid.

In order to confirm this scenario, we calculate the structure function $S(\mathbf{k})$ at various temperatures, and display the resulting intensity plots in Fig. 16. We clearly see the pinned solid [Fig. 16(a)], the floating solid [Fig. 16(b)], and the liquid [Fig. 16(c)] phases. It is interesting to note that the rotational symmetry of the pinned and floating solids breaks the fourfold rotational symmetry of the square grid, leading to two possible degenerate orientations. In the liquid, however, we see that the fourfold symmetry of the square grid is restored, with a strong fourfold angular modulation of the circular intensity peaks. This observation is also confirmed by a direct measurement of $\varphi_4(T)$ [see Fig. 14(b)], which is close to zero in the floating solid phase, but then rises sharply at the melting transition and only slowly vanishes with increasing temperature. The small values of $\varphi_4(T)$ for $T_c(f) < T < T_m$ are an indication of the extent to which the commensurate, slightly distorted triangular lattice of the ground state, beomes an incommensurate perfect triangular lattice in the floating solid phase.

Since we are unable to carry out finite-size scaling, we are unable to search in detail for the hexatic phase, or for the predicted[20] Ising transition from the hexatic to the normal liquid. However, as the fourfold symmetry appears to be restored at the same temperature as the melting transition, we suggest that, as was found for the triangular grid, the hexatic phase is absent and the melting transition is first order.

Although finite-size scaling is not possible, we can nevertheless still obtain the translational correlation exponent $\eta_{\mathbf{G}_1}$ by analyzing the decay of the peaks in the structure function, using the method discussed in connection with Eqs. (23)–(25). In the present case the implementation of this method is somewhat trickier than it was for the triangular grid, since, due to the incommensurabil-

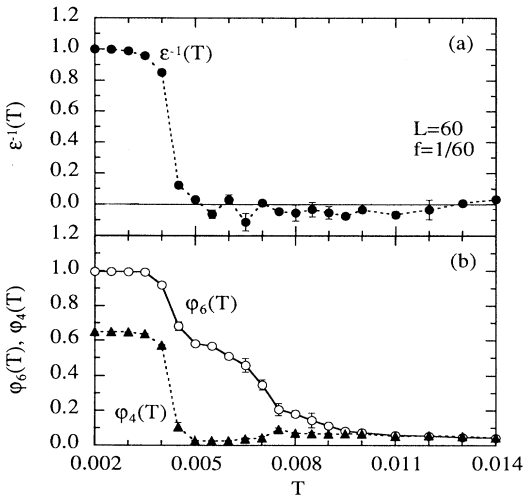

FIG. 15. (a) Inverse dielectric constant $\epsilon^{-1}(T)$ and (b) orientational correlations $\varphi_6(T)$ and $\varphi_4(T)$ versus T, for the system with nearly triangular ground state with $f = 1/60$ and $L = 60$.

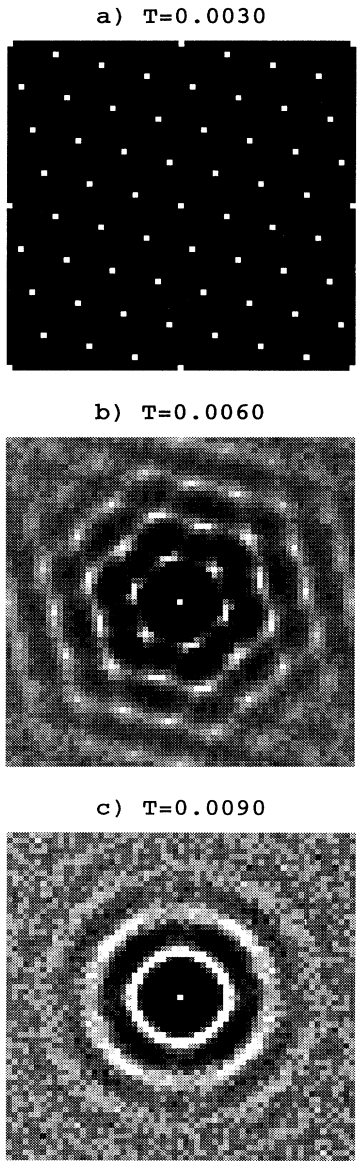

FIG. 16. Melting of a nearly triangular vortex lattice on the square grid. Intensity plots of $S(\mathbf{k})$ for $f = 1/60$, $L = 60$, and several temperatures: (a) $T = 0.003$ in the pinned solid, (b) $T = 0.006$ floating solid, (c) $T = 0.009$ in the liquid.

ity of the floating solid, the peaks in $S(\mathbf{k})$ do not have well-defined positions $\mathbf{G}$ on the square reciprocal lattice. We overcome this difficulty by numerically scanning $S(\mathbf{k})$ for local maxima at a given distance from the center of the reciprocal lattice, and averaging over the heights of peaks of the same order. The peak heights estimated in this way are shown in Fig. 17 for several temperatures T in the floating lattice phase. Dashed lines are least squares fits to the formula (24), and the extracted exponents $\eta_{\mathbf{G}_1}(T)$ are summarized in Table III. The accuracy of the fit appears to be as good as in the case of the triangular grid, and we therefore have good reason to believe that our determination of $\eta_{\mathbf{G}_1}(T)$ (and thus the vortex shear modulus μ) is reasonably accurate. Once again we see from Table III that $\eta_{\mathbf{G}_1}(T)$ first exceeds the universal KT value of 1/3 at $T \simeq 0.007$, very close to the melting temperature $T_m \simeq 0.0075$ estimated from the behavior of $\varphi_6(T)$.

C. Systems with "nearly square" ground state: $f = 1/51$

We now briefly describe our results from simulations on a system with density $f = 1/51$, which possesses a nearly square ground state [Fig. 14(b)]. Our results are for a system of size $L = 51$. The temperature dependence of the inverse dielectric function $\epsilon^{-1}(T)$ is shown in Fig. 18(a). From the data, we estimate the depinning temperature to be $T_c(f) \simeq 0.0035$. We note that even though $f = 1/51$ here is larger than the $f = 1/60$ studied in the previous section, we find $0.0035 = T_c(1/51) < T_c(1/60) = 0.0045$, thus illustrating the nonmonotonic behavior of $T_c(f)$ for small f. The significantly lower depinning temperature in the present case may be qualitatively understood as a result of the larger distortion of the ground state away from the perfect triangular lattice favored by the vortex-vortex interaction. This large distortion, which is favored by the pinning energy, comes at a cost in vortex-vortex interaction energy. The result is a reduced free energy difference between the pinned "distorted triangular" solid and the perfect triangular floating solid, and hence a reduced depinning temperature. A similar observation

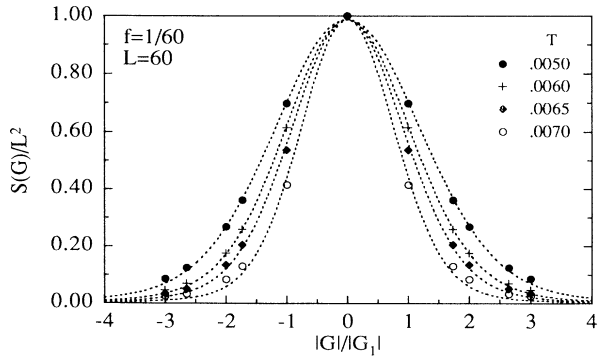

FIG. 17. Heights of the peaks $S(\mathbf{G})$ versus $|\mathbf{G}|$ for $f = 1/60$ and $L = 60$. Dashed lines represent the best fit to Eq. (24), and are used to extract the exponent $\eta_{\mathbf{G}_1}(T)$.

TABLE III. Temperature dependence of the exponents $\eta_{\mathbf{G}_1}(T)$ of the floating vortex lattice on the square grid as obtained by fitting the height of peaks in the structure function, for $f = 1/60$ and $L = 60$.

T	$\eta_{\mathbf{G}_1}(T)$
0.0040	0.0024±0.001
0.0045	0.111 ±0.016
0.0050	0.198 ±0.012
0.0055	0.224 ±0.009
0.0060	0.270 ±0.011
0.0065	0.33 ±0.04
0.0070	0.49 ±0.10

holds for the other values of f we have studied: Systems with relatively lower $T_c(f)$ compared to other nearby values of f are those with greater distortion of the ground state from a triangular lattice.

In Fig. 18(b) we plot the temperature dependences of the fourfold and sixfold orientational correlations $\varphi_4(T)$ and $\varphi_6(T)$. In contrast to the previously considered cases, the melting transition is barely visible here: One sees only a small kink in $\varphi_4(T)$ and an inconspicuous dip in $\varphi_6(T)$ near $T = 0.005$. For a clearer picture of melting, we show the structure function $S(\mathbf{k})$ in Fig. 19. We see again the pinned solid [Fig. 19(a)], the floating solid [Fig. 19(b)], and the liquid [Fig. 19(c)]. Note that the peaks in the floating solid occur at distinctly different wave vectors $\mathbf{k}$ than in the pinned solid; this emphasizes the fact that $T_c(f)$ is truly a transition from a commensurate "nearly square" lattice, to an incommensurate floating triangular lattice. Inspection of these intensity plots gives a melting transition of $T_m \simeq 0.005$, in agreement with the value hinted at in Fig. 18(b). We note that this value is significantly lower than the value of 0.007 found in other cases. Thus commensurability effects can also significantly lower the melting temperature. Such com-

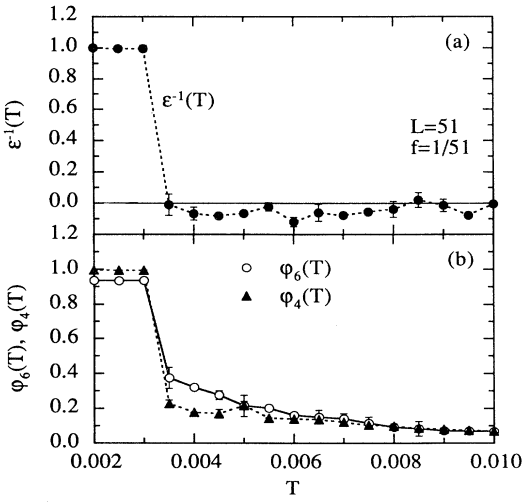

FIG. 18. (a) Inverse dielectric constant $\epsilon^{-1}(T)$ and (b) orientational correlations $\varphi_6(T)$ and $\varphi_4(T)$ versus T, for the system with nearly square ground state with $f = 1/51$ and $L = 51$.

mensurability effects presumably become less significant as f decreases and the ground state becomes increasingly closer to a triangular lattice. We thus expect that the melting temperature becomes $T_m \simeq 0.007$ in the asymptotic $f \to 0$ limit, as is indeed suggested by Fig. 13.

V. SIMULATIONS ON THE SQUARE GRID: NEAR FULL FRUSTRATION

The square superconducting network with $f = 1/2$ has been the focus of extensive theoretical study in recent years.[9,10,36] As the Hamiltonians, Eqs. (1) and (5), are periodic in f with period 1, $f = 1/2$ represents the strongest magnetic field, and most dense vortex configuration, discernable by the network. Thus this case is usually referred to as "fully frustrated." The ground state of this configuration is in some sense the simplest of all $f > 0$, consisting of a checkerboard pattern of vortices, with $n_i = 1$ and $n_i = 0$ on the two alternating sublattices of the square grid. This dense vortex lattice melts[10] directly into a vortex liquid at $T_m(1/2) \simeq 0.13$. Superconducting coherence vanishes[40] at $T_c(1/2) \simeq T_m(1/2)$.

We now wish to study how the system behaves as f is varied slightly away from 1/2, in order to test the discontinuous behavior predicted by the TJ conjecture. We study in particular systems with $f = 1/2 - 1/q$, with integer q large. While the ground states for densities of this form have been studied by Straley and co-workers,[7,41] finite-temperature properties have remain unexplored.

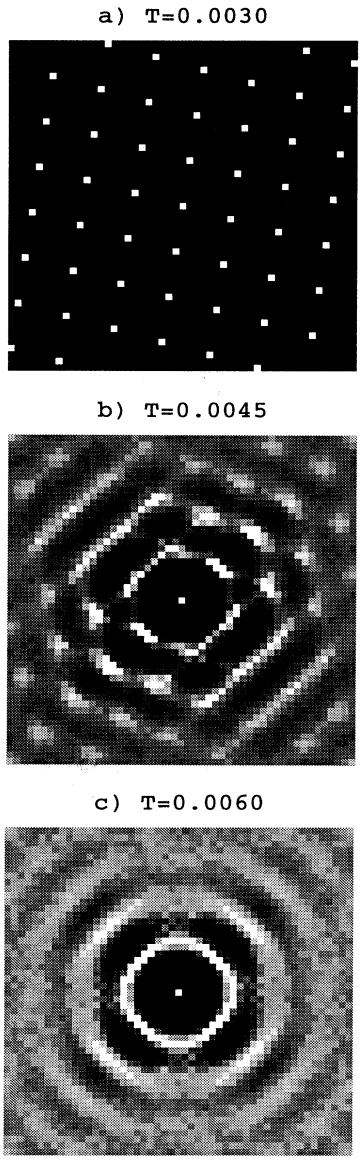

FIG. 19. Melting of a nearly square vortex lattice on the square grid. Intensity plots of $S(\mathbf{k})$ for $f = 1/51$, $L = 51$, and several temperatures: (a) $T = 0.003$ in the pinned solid, (b) $T = 0.0045$ in the floating solid, (c) $T = 0.006$ in the liquid.

A. $f = 5/11$

We first consider the particular case of $f = 5/11$, which may be written as $f = 1/2 - 1/22$. The correct ground state for this case, which we show in Fig. 20, was first found by Kolachi and Straley.[41] It consists of a periodic superlattice of vortex vacancies superimposed on an otherwise uniform $f = 1/2$ like background, and is periodic with a 22×22 unit cell. Our motivation is to see whether or not this superlattice of vacancies (or "defects") can melt independently of the $f = 1/2$ like background, and if so, whether the resulting liquid of vacancies destroys superconducting coherence. Our analysis is similar to that in the previous section.

Heating from the ground state, we show sample intensity plots of the structure function $S(\mathbf{k})$, at different temperatures, in Fig. 21. Figure 21(a) shows the low-temperature phase at $T = 0.010$. The bright Bragg peaks at $\mathbf{k} = (\pm\pi/a_0, \pm\pi/a_0)$ originate from the vortex ordering in the $f = 1/2$ like background, while the pe-

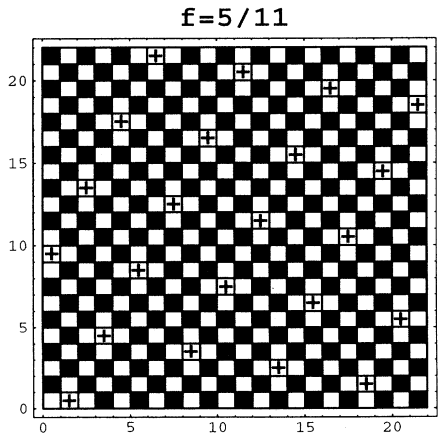

FIG. 20. Ground state for $f = 5/11$ on a 22×22 unit cell. Solid squares represent vortex positions. Crosses (+) indicate vacancies (defects) in the otherwise perfect checkerboard pattern of $f = 1/2$.

riodic Bravais lattice of less intense Bragg peaks is due to the defect superlattice, which at this low temperature is pinned to the substrate. Thus we have a "pinned defect solid" phase. As the temperature is increased, we find that the defect superlattice melts at $T_m \simeq 0.015$. In Fig. 21(b) we show the system at $T = 0.018$, just above this melting. The defects no longer give rise to Bragg peaks, but instead we see the circular rings (with strong fourfold angular modulation) characteristic of a defect liquid. However, the bright Bragg peaks at $\mathbf{k} = (\pm\pi/a_0, \pm\pi/a_0)$ remain, indicating that the $f = 1/2$ like vortex background remains ordered. Upon increasing the temperature further, the ordered $f = 1/2$ background is also eventually destroyed at $T_{m'} \simeq 0.040$. In Fig. 21(c) we show the system at $T = 0.055$, above $T_{m'}$. The peaks at $\mathbf{k} = (\pm\pi/a_0, \pm\pi/a_0)$ have broadened to finite width, indicating the disordering of the $f = 1/2$ like background.

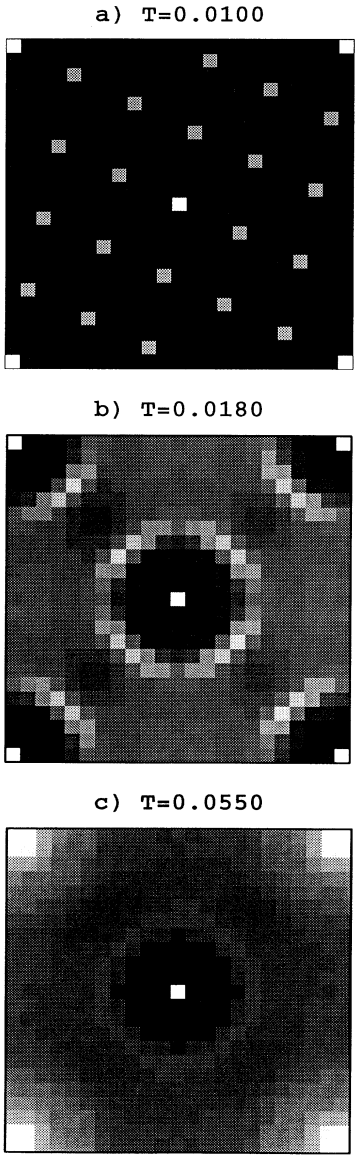

FIG. 21. Melting of $f = 5/11$ for $L = 22$. $S(\mathbf{k})$ is shown for (a) $T = 0.010$ in the pinned defect solid, (b) $T = 0.018$ in the defect liquid, (c) $T = 0.055$ in the completely disordered high-temperature phase.

To see the melting transitions more clearly, in Fig. 22 we plot versus temperature the peak heights $S(\mathbf{q}^*)$ and $S(\mathbf{G}_1)$, with $\mathbf{q}^* \equiv (\pi/a_0, \pi/a_0)$ giving the ordering of the $f = 1/2$ like background, and $\mathbf{G}_1$ the shortest reciprocal lattice vector of the defect superlattice. We see that $S(\mathbf{G}_1)$ vanishes sharply at $T_m \simeq 0.015$, where the pinned defect superlattice melts into a defect liquid. $S(\mathbf{q}^*)$, however, remains at its $T = 0$ value of unity for all temperatures up to $T \simeq 0.020$, clearly demonstrating that the $f = 1/2$ like vortex background remains ordered throughout the defect melting transition. $S(\mathbf{q}^*)$ starts to drop to zero around $T_{m'} \simeq 0.04$, where, based on the structure function intensity plots, we have estimated that the $f = 1/2$ like background melts.

To investigate superconducting coherence, in Fig. 23 we show the inverse dielectric function versus temperature. We see that ϵ^{-1} vanishes at the defect melting transition T_m. The diffusing defects above T_m induce a diffusion of vortices, which must move to fill in the "hole" left behind by the defect as it moves. The diffusing vortices are then responsible for the destruction of superconducting phase coherence.

To summarize, we have found clear evidence that the introduction of a small concentration of defects into the fully frustrated system results in a dramatic decrease of the superconducting transition temperature from its $f = 1/2$ value. The fluctuations of the defect superlattice, on an essentially frozen $f = 1/2$ like background, result in behavior which is in many respects like that of the dilute vortex lattices studied in Sec. IV. In the present case, we find that the defect superlattice melts directly from a pinned solid into a liquid. In the following section we will argue, following the analogy with Sec. IV, that a more dilute defect superlattice would first unpin at a $T_c(f)$ into a floating defect superlattice, which would then melt at a higher temperature T_m into a defect liquid.

The sharp melting transition of the $f = 1/2$ like background at a temperature $T_{m'}$ distinctly higher than the

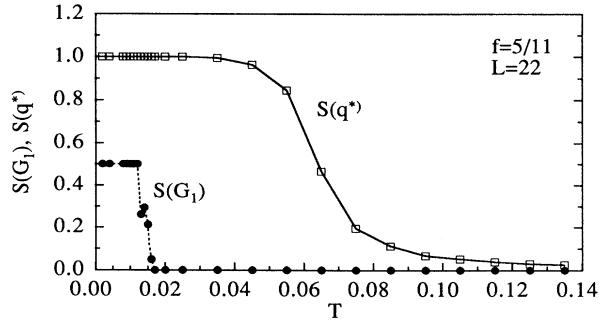

FIG. 22. Peak heights $S(\mathbf{q}^*)$ with $\mathbf{q}^* \equiv (\pi/a_0, \pi/a_0)$, and $S(\mathbf{G}_1)$ where $\mathbf{G}_1 = (2\pi/L)(1, 5)$ is the shortest reciprocal lattice vector of the defect superlattice, plotted versus T for $f = 5/11$ and $L = 22$.

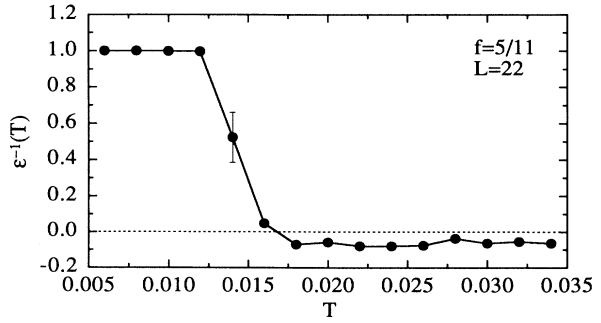

FIG. 23. Inverse dielectric constant $\epsilon^{-1}(T)$ versus T for $f = 5/11$ and $L = 22$.

defect melting at T_m is a new phenomenon, with no analog in the dilute small f systems (at small f there is only a smooth crossover remnant of the vortex-antivortex unbinding transition of the $f = 0$ case). From symmetry, one would expect that the transition at $T_{m'}$ is of the Ising type. Undersanding whether the melting transition in the pure $f = 1/2$ case is Ising like or not has been the subject of much work, with the most recent simulations suggesting that it is not;[10] if it is not Ising, this is most likely due to the long-range nature of the vortex interactions. For the $f = 5/11$ case, however, the melted defect liquid will serve to screen the interactions of the vortices in the $f = 1/2$ like background, resulting in effectively short-ranged interactions. An Ising transition is therefore most probable. We are unable to test this prediction, as we are unable to carry out a detailed finite-size scaling analysis, for the same reasons as discussed in Sec. IV. However, the strong screening effect of the defect liquid is evident in the substantial reduction of the background melting temperature, $T_{m'}(5/11) \simeq 0.04$, as compared to the melting transition $T_m(1/2) \simeq 0.13$ of the pure $f = 1/2$ case.

B. General case: $f = 1/2 - 1/q$

In this section, we strengthen the analogy between the melting of the defect superlattice seen in the previous section, with the melting of the dilute (small-f) vortex lattices studied in Sec. IV, in order to discuss the general case of $f = 1/2 - 1/q$. Our goal is to establish that for a more dilute density of defects one will have a floating defect solid intermediate between a pinned defect solid and a defect liquid.

As seen for the $f = 5/11$ case, throughout a temperature range including the defect lattice melting transition T_m, the $f = 1/2$ like background vortices remain perfectly ordered as at $T = 0$; domain excitations, which would reduce $S(\mathbf{q}^*)$ from its $T = 0$ value of unity, become important only above T_m. In this case, one can focus solely on excitations which are due to the motion of the defects. At $T = 0$, these defects are seen to sit on the same sublattice of the square grid as do the $n_i = 1$ vortices of the $f = 1/2$ like background (see Fig. 20); equivalently, one never has two vortices on two nearest neighbor sites. We assume that this restriction continues to hold at finite temperatures up to and including T_m; i.e., the cost in energy to have two vortices on nearest neighbor sites is so high compared to T_m, that such excitations may be ignored.

With this assumption, we have reduced our problem at $f = 1/2 - 1/q$ to that of a density $1/q$ of logarithmically interacting defects, which are restricted to move on only one of the two sublattices of the original square grid. This sublattice is itself a square lattice of lattice constant $\sqrt{2}a_0$. As the sublattice has half the number of sites as in the original grid, our problem is thus effectively the same as a dilute density $f' = 2/q$ of vortices on a square grid. This mapping would be exact (within our assumptions) except for the fact that the interaction potential $V(\mathbf{r})$ between the defects is still defined with respect to the original square grid, and not the sublattice to which the defects are constrained. However, as q gets large, and the average spacing between defects becomes much greater than a_0, we expect that this difference will be a negligible effect.

The assumption that the defects move only on one sublattice can be checked for the $f = 5/11$ case of the previous section. Restricting the defects in real space to a sublattice whose unit cell has twice the area of that of the orginial square grid, means that the first Brillouin zone of the effective reciprocal lattice is reduced by a factor of $\frac{1}{2}$. Instead of the square-shaped BZ shown in Fig. 21, the effective BZ is now an inscribed diamond whose vertices bisect the edges of the squares of Fig. 21. The structure function $S(\mathbf{k})$, as plotted over the full square-shaped BZ of the original square grid, should now just be obtained by a periodic repetition of the diamond-shaped BZ corresponding to the sublattice. Such periodicity is clearly seen in Figs. 21(a) and 21(b), for both the pinned defect solid and the melted defect liquid. It is absent in Fig. 21(c), where $T > T_{m'}$, and the $f = 1/2$ like background has melted.

Having checked the validity of our assumption for $f = 5/11$, we note that it should be even better satisfied for more dilute defect densities $f = 1/2 - 1/q$, $q > 22$. As q increases, the density of defects decreases, resulting a reduced screening of the interactions between the background vortices. The background melting temperature $T_{m'}$ should therefore increase and approach its higher $f = 1/2$ value. At the same time, the defect superlattice unpinning temperature T_c should decrease as $\sim 1/q$, while the defect superlattice melting temperature T_m saturates to a lower fixed value. Thus we expect that the window of temperatures in which our assumption is valid becomes wider as q increases.

We can now understand the behavior found in the preceding section. For $f = 5/11 = 1/2 - 1/22$, we have $q = 22$, and so the defects behave like an effective vortex density of $f' = 2/q = 1/11$. Comparing to our results of Fig. 13 in Sec. IV, we see that f' is large enough that we expect only a direct melting of the pinned defect solid to a defect liquid, consistent with our observation in the preceding section. In order to observe a floating defect solid, we will have to consider an $f' < 1/30$, or an $f = 1/2 - 1/q$ with $q > 60$.

To simulate a system with $f = 1/2 - 1/60$ directly, would require a grid size of at least $L = 60$, with $N_c = 1740$ vortices. This is beyond our present computational ability ($f = 5/11$, with $L = 22$ and $N_c = 220$, is about the largest system we can manage). However, our conclusion, that at temperatures low compared to $T_{m'}$ the defects move in the presence of an effectively frozen $f = 1/2$ like background, allows us to construct a much more efficient algorithm which will be suitable for describing behavior up to and above the defect melting transition T_m, provided we stay below the background melting transition $T_{m'}$. We do this by fixing the $f = 1/2$ like background and allowing only the vacancies to move around. This significantly reduces the number of degrees of freedom in the simulation, and we shall thus be able to treat systems with a much smaller fraction of defects $1/q$, than we could by direct MC simulation.

In order to implement the algorithm suggested above, we formally decompose the charge at site $\mathbf{r}_i$ into two parts

$$n_i = s_i - \delta n_i, \tag{33}$$

where

$$s_i \equiv \frac{1}{2}[1 + (-1)^{x_i+y_i}] = \frac{1}{2}(1 + e^{i\mathbf{r}_i\cdot\mathbf{q}^*}) \tag{34}$$

is the staggered pattern of the background vortices [$\mathbf{q}^* \equiv (\pi/a_0, \pi/a_0)$] and δn_i are new integer variables representing the defects in the background. Neutrality requires that $\sum_i \delta n_i = L^2/q$. Substituting Eq. (33) for n_i in the Hamiltonian (5), we get

$$\mathcal{H} = \frac{1}{2}\sum_{ij} \delta n_i V'_{ij} \delta n_j - \sum_{ij} \delta n_i V'_{ij}(s_j - f) + \frac{1}{2}\sum_{ij}(s_i - f)V'_{ij}(s_j - f), \tag{35}$$

where $V'_{ij} \equiv V'(\mathbf{r}_i - \mathbf{r}_j)$. The first term in the Hamiltonian (35) gives the interaction between defects; the second term represents the interaction of the defects with a one-body potential,

$$\Phi_i \equiv \sum_j V'_{ij}(s_j - f)\,, \tag{36}$$

created by the background; the last term is just an additive constant. Substituting Eq. (34) for the s_i into Eq. (36) above, gives the potential Φ_i in terms of the Fourier components of the interaction, $V_{\mathbf{k}}$,

$$\Phi_i = \frac{1}{2}V_{\mathbf{q}^*}e^{i\mathbf{r}_i\cdot\mathbf{q}^*} - \left(\frac{1}{2} - f\right)\sum_{\mathbf{k}\neq 0} V_{\mathbf{k}}, \tag{37}$$

where from Eq. (7) we have $V_{\mathbf{q}^*} = \pi/4$. Thus Φ_i oscillates with the same checkerboard pattern of the $f = 1/2$ like background. Comparing with Eq. (34), we see that the Hamiltonian of Eq. (35) can now be rewritten in the following simple form

$$\mathcal{H} = \frac{1}{2}\sum_{ij} \delta n_i V'_{ij} \delta n_j - \frac{\pi}{4}\sum_i \delta n_i s_i + E_0, \tag{38}$$

where E_0 is an additive constant.

So far, the formulation above is exact. Our approximation that the background is frozen, and that defects only move on the sublattice defined by $s_i = 1$, occurs when we consider only the case where N_c sites have the value $\delta n_i = 1$, and all other sites have $\delta n_i = 0$. In this approximation, the Coulomb gas near full frustration, $f = 1/2 - 1/q$, is equivalent at low temperatures to the dilute Coulomb gas of defects with integer charges $\delta n_i = 0, 1$, moving in a staggered potential of magnitude $\delta\Phi = \pi/4 = 0.7853\ldots$. As this magnitude is about two orders of magnitude greater than the relevant excitation energy scale, set by temperature T_m, the sites with $\delta n_i = 1$ are essentially restricted to the sublattice where $s_i = 1$; in this case they represent the vacancies in the $f = 1/2$ like background. The case where $\delta n_i = 1$ on the opposite sublattice where $s_i = 0$ represents a $(+1, -1)$ vortex-antivortex excitation, which can be ignored on energtic grounds as we had shown in earlier sections.

To check the consistency of the above procedure, we have redone our simulation of $f = 5/11$ using the new algorithm based on the Hamiltonian (38). In a fraction of the CPU time needed for the original simulation using the full Hamiltonian (5), we have recovered our original results for all quantities, at all temperatures up to about $T \simeq 0.040$, where fluctuations in the $f = 1/2$ background become significant.

Having verified the consistency of the new algorithm in this way, we now proceed to simulate systems with more dilute concentrations of defects. In Fig. 24, we display the structure function $S(\mathbf{k})$ for the case $f = 22/45 = 1/2 - 1/90$. As expected from the discussion above, we observe a clear signature of the floating solid phase [Fig. 24(b)] in the temperature range $0.005 < T < 0.008$. This range is identical to the range in which we found the floating solid phase for $f' = 1/45$ (see Fig. 13). The low-temperature phase is a familiar "pinned defect solid" [Fig. 24(a)]; the high-temperature phase is a defect liquid with strong fourfold correlations [Fig. 24(c)]. The above scenario is confirmed by a direct measurement of $\epsilon^{-1}(T)$ and the sixfold orientational correlation $\varphi_6(T)$ of the defects δn_i, shown in Fig. 25. Both quantities behave in a way similar to those measured for dilute vortex systems, showing a sharp drop in $\epsilon^{-1}(T)$ at the depinning transition, and a plateau in $\varphi_6(T)$ in the floating phase.

To summarize, we conclude that for $f = 1/2 - 1/q$, with $q > 60$, there will be the following sequence of transitions. At low temperature there is a pinned superlattice of defects of density $1/q$, which unpins at $T_c(f) \sim 2/q$ into a floating superlattice of defects. This floating lattice melts at $T_m \simeq 0.007$ into an isotropic defect liquid. Finally, at $T_{m'}$, which approaches the value of 0.13 as q increases, the $f = 1/2$ like background melts via an Ising transition, resulting in an isotropic vortex liquid of density f.

VI. SUMMARY AND CONCLUSIONS

We have carried out extensive Monte Carlo simulations of the Coulomb gas Hamiltonian (5) as a model of a 2D

superconducting network in an external transverse magnetic field. One of the goals of our work was to systematically study, for the special cases of vortex density $f = 1/q$ and $f = 1/2 - 1/q$ ($q \gg 2$), a conjecture put forward by Teitel and Jayaprakash,[5] that for $f = p/q$ the superconducting transition temperature scales approximately as $T_c(f) \sim 1/q$. For the dilute case, $f = 1/q$, we have found good agreement with this conjecture, provided one interprets the superconducting transition temperature to be the vortex-lattice unpinning temperature $T_c(f)$, where the ground state vortex lattice decouples from the superconducting network, and is free to slide transversly to any applied dc current, thus producing "flux flow" resistance.

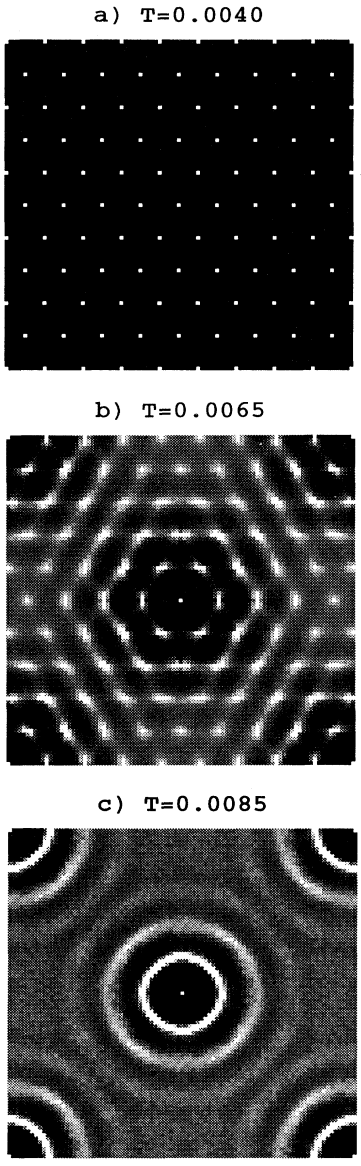

FIG. 24. Melting of the defect superlattice for $f = 22/45$ and $L = 90$. Intensity plot of $S(\mathbf{k})$ for (a) $T = 0.0040$ in the pinned defect solid, (b) $T = 0.0065$ in the defect floating solid, (c) $T = 0.0085$ in the defect liquid. Intensities at $(\pm\pi/a_0, \pm\pi/a_0)$ and $(0,0)$, which arise from the fixed staggered background, have been substracted for the sake of clarity.

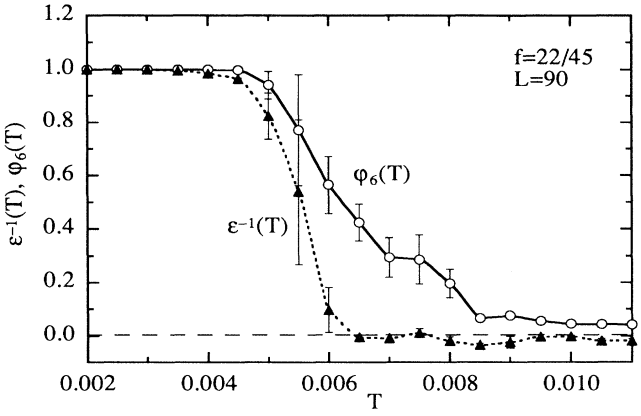

FIG. 25. Inverse dielectric function $\epsilon^{-1}(T)$ and orientational correlation $\varphi_6(T)$ versus T, for $f = 22/45$ and $L = 90$.

A new result of our work is the realization that above $T_c(f)$, for sufficiently dilute systems, a depinned "floating" vortex solid will exist. This floating vortex solid has essentially the same properties as a vortex lattice in a uniform superconducting film, and it melts (as $q \to \infty$) at $T_m \simeq 0.007$ into an isotropic vortex liquid. While the true onset of finite linear dc resistivity will be $T_c(f)$, the melting at T_m is presumably accompanied by a sharp rise in resistivity. The distinction between T_c and T_m, however, may be difficult to observe experimentally, due to the existence of large energy barriers[14] for the hopping of a vortex between neighboring cells of the superconducting network. As discussed in the Introduction, the discrete nature of the network introduces an effective periodic pinning potential for vortices. For a square Josephson array, Lobb *et al.*[14] have estimated the energy barrier of this pinning potential to be $E_b \simeq 0.199/2\pi = 0.0317$ (in our energy units[42]). This is almost 5 times the vortex-lattice melting temperature $T_m \simeq 0.007$. Thus, for the square network, one is most likely to observe upon cooling only a vortex liquid, in which the vortex mobility decreases exponentially as $e^{-E_b/T}$; the true phase transitions at T_m and T_c will be masked by the extremely slow relaxation over the energy barriers E_b at these low temperatures. Such behavior has in fact been reported[15,43] in experimental studies of square Josephson arrays, where for small f near $f = 0$, only exponentially decreasing resistive tails are observed at low temperature; no evidence for the melting or depinning transitions at T_m and T_c has been found. For the triangular Josephson array, however (a case we have not explicitly studied here), the energy barrier is estimated[14] to be $E_b \simeq 0.0427/2\pi = 0.0068$ (in our energy units). This is comparable to T_m, and so there might be some slight chance of experimentally observing the melting transition. Recent experimental studies of this system[44] at small f have found surprising dynamical behavior, indicating anomalously slow diffusion of vortices. However, the temperature of these experiments, $T \simeq 0.5T_c(f = 0)$, appears to be too high for these results to be explained by any of the melting or depinning effects we have found here. For a honeycomb

Josephson array (vortices on a triangular grid) we estimate the highest barrier,[45] with $E_b \simeq 0.751/2\pi = 0.119$.

For dense systems close to full frustration, $f = 1/2 - 1/q$, we have argued that, at temperatures low compared to the melting temperature of the pure $f = 1/2$ system, the physics is dominated by defects moving on top of a quenched $f = 1/2$ like vortex background. We have shown how this system of defects can be mapped onto the dilute Coulomb gas of vortices with density $f' = 2/q$. The resulting behavior is then obtained from knowledge of this dilute limit. The TJ conjecture again holds, with $T_c[f = (q-2)/2q] \sim 2/q$ marking the transition from a pinned defect superlattice to a floating defect superlattice, in which true dc superconductivity is lost. At a higher $T_m \simeq 0.007$, the floating defect solid melts into an isotropic defect liquid. At yet a higher $T_{m'}$, the $f = 1/2$ like background disorders. As in the $f = 0$ case, the transitions at T_c and T_m may be difficult to observe experimentally, due to the energy barrier for a defect to hop between nearest neighbor sites of the relevant sublattice. For a square lattice, Dang and Györffy[46] have estimated this barrier to be $E_b \simeq 0.368/2\pi$ (in our energy units), even larger than that found for $f = 0$. Experimental studies[15,47] of square Josephson arrays for f near $f = 1/2$ have again found only exponential resistive tails as the temperature decreases.

In contrast to the transitions at T_c and T_m, we expect that the sharp disordering transition of the $f = 1/2$ like background at $T_{m'}$ should be experimentally observable. This follows since for $f = 1/2 - 1/q$, we expect that as $q \to \infty$, $T_{m'} \to T_m(1/2) \simeq 0.13$, well above the energy scale of the barriers. This transition would presumably manifest itself as a singular increase in the linear resistivity at $T_{m'}$ (from an already finite value). The phase boundary $T_{m'}(f)$ near $f = 1/2$ is presumably a smooth funtion of the defect density, $1/2 - f$; however, we are unable to estimate it due to our inability to simulate sufficiently large systems.

Our mapping between a dilute density of defects near $f = 1/2$, and a dilute vortex density near $f = 0$, may be extended to the more general case. Using the same arguments as in Sec. V, we would expect that the system with $f = 1/2 - p/q$, with p/q sufficiently small, should have the same low-temperature behavior as the density $f' = 2p/q$. For p/q sufficiently small, we would expect that the dilute vortex lattice of density $f' = 2p/q$ behaves qualitatively like those of density $1/q$ studied here; i.e., there is first a depinning transition at $T_c(f)$ which decreases as p/q decreases (whether it vanishes as p/q or as $1/q$ remains to be investigated) followed by a melting transition at $T_m \simeq 0.007$. Thus for any rational fraction sufficiently close to either $f = 0$ or $f = 1/2$, we would expect behavior similar to the cases explicitly studied here.

We thus see that the TJ conjecture appears to hold, according to the following scenario. Consider a vortex density f close to some simple fraction $f_0 = p_0/q_0$, $f = f_0 - 1/q$, with $q_0 \ll q$. The ground state is one which is almost everywhere like that of f_0, except for a pinned periodic superlattice of defects of density $1/q$. If q is sufficiently large, this superlattice will unpin into a floating defect solid at $T_c(f) \sim 1/q$. Defects which are free to move lead to flux flow resistance, and destroy the superconducting phase coherence of the system. Thus an arbitrarily small concentration of defects added on top of the f_0 like background (i.e., for f arbitrarily close to f_0) dramatically decreases the superconducting transition temperature, when compared to the pure f_0 system. We have explicitly tested this scenario for the cases $f_0 = 0$ and $f_0 = 1/2$. We speculate that this behavior will be characteristic of systems near any simple fraction $f_0 = p_0/q_0$. We further speculate that this behavior may be characteristic for *any* sufficiently small rational fraction of defects away from a simple fraction f_0, i.e., $f = p_0/q_0 - p/q$ with $q_0 \ll q$.

A second goal of our work was to study in detail the melting transition of the 2D vortex lattice. This problem has been addressed previously only in the context of uniform superconducting films. Here we have addressed this issue in the context of a superconducting network. We believe, however, that our results for the dilute case we have studied in Sec. III are representative of the continuum limit, as treated within the London approximation. Melting within this London approximation has been treated theoretically by Huberman and Doniach,[31] and Fisher,[32] who applied the KTNHY theory of defect mediated melting in 2D. This theory predicts a second-order melting transition at a T_m well below the Ginzburg-Landau mean field transition temperature $T_{\rm MF}$, as well as an intermediate hexatic liquid phase. We have carried out the first detailed finite-size scaling analysis to check this KTNHY theory as applied to vortex-lattice melting. We find a value $T_m \simeq 0.007 \pm 0.0005$ in good agreement with the value estimated by Fisher. We also find that the vortex-lattice shear modulus jumps discontinuously to zero at T_m, with a value close to the KTNHY prediction. However, we find that the melting transition is weakly first order, and we find no evidence for a hexatic phase. Our value for T_m and our conclusion concerning the order of the melting transition are in agreement with earlier simulations[48] of the continuum one-component plasma model of Eq. (13).

This problem of 2D vortex-lattice melting has been the focus of much renewed work recently, due to its potential connection with behavior in anisotropic high-temperature superconductors. The very existence of a vortex lattice at any finite temperature has been challenged by Moore,[4] who argued that fluctuations in the phase of the order parameter $\psi(\mathbf{r})$, due to shear excitations of the vortex lattice, will cause the order parameter correlation function $\langle \psi^*(\mathbf{r})\psi(0)\rangle$ to decay exponentially at any finite temperature. From such decay, Moore argued first for the absence of a superconducting state, and then concluded as a result of this absence of superconductivity that the vortex lattice should not exist. Support for this scenario is suggested by high-temperature perturbative expansions, which also find no evidence for freezing into a vortex lattice, even when evaluated to high order.[49]

Recently, simulations have been carried out to address this question. In contrast to our work in the London approximation, these works have been carried out in the so-called lowest-Landau-level (LLL) approximation,

which is based on the Ginzburg-Landau (GL) free energy $\mathcal{H}_{GL}$ of Eq. (11). In this approximation, the complex order parameter $\psi(\mathbf{r})$ is expanded in terms of the lowest degenerate eigenstates of the Gaussian part of the Ginsburg-Landau free energy, and the coefficients of this expansion (or alternatively the complex positions of the vortices) are used as fluctuating variables in a Monte Carlo simulation with $\mathcal{H}_{GL}$ as the Hamiltonian. Using such simulations, and modeling a 2D system by the surface of a sphere, O'Neill and Moore[50] failed to find evidence for a vortex lattice. Other simulations in a 2D plane, however,[51–54] reported clear evidence for the melting of a vortex lattice at a finite temperature. Hu and MacDonald[52] and Kato and Nagaosa[53] find that this melting transition is weakly first order, in agreement with our London result. Šášik and Stroud[54] similarly find a first-order transition; they further compute the vortex-lattice shear modulus μ and find behavior at T_m in agreement with our result. Most recently, Herbut and Tešanović[55] have developed a density functional theory of the vortex lattice melting transition, based on the LLL formalism. They again find results consistent with the above, for the order of the transition, and the shear modulus μ.

Thus, with the exception of Ref. 50, results from the London and LLL approximations seem to be in agreement. This is as one might expect from the principle of universality in phase transitions. Although the London approximation at the "microscopic" level ignores fluctuations in the amplitude of $\psi(\mathbf{r})$ (such as are included in the LLL formalism), upon coarse graining the London model, phase fluctuations at the microscopic length scale will generate amplitude fluctuations on the coarse-grained length scale. On this coarse-grained scale, the system will be described by some effective Ginzburg-Landau free energy, complete with amplitude fluctuations, although higher-order terms in ψ beyond those given in Eq. (11) may be present. In contrast to the London approximation, the Ginzburg-Landau free energy of Eq. (11) includes amplitude fluctuatons at the "microscopic" scale, and it is thus often viewed as a more fundamental description. However, the GL form of Eq. (11) represents only the lowest terms in an expansion of the free energy in powers of $|\psi|$, and hence is valid only near the mean field transition T_{MF} where $|\psi|$ is small. Since vortex-lattice melting occurs at $T_m << T_{MF}$, higher-order terms in ψ may well be important for a quantitative description. These higher-order terms, however, are presumably irrelevent in determining the critical behavior, thus leading to agreement between the London and LLL simulations.

Note added in proof: Recent simulations[57] for small f within the θ representation of Eq. (1) have been reported by Hattel and Wheatley. Their results are consistent with those reported here. These authors have also reported[58] a theoretical argument for the linear dependence $T_c(f) \sim f$, at small f. Similar results were earlier found by Martinoli *et al.*[59] for a 2D vortex lattice in a one-dimensional periodic pinning potential.

ACKNOWLEDGMENTS

The authors are grateful to T. Chen, D. A. Huse, D. R. Nelson, and Z. Tešanović for helpful discussions. This work was supported by DOE Grant No. DE-FG02-89ER14017.

[1] For a review, see *Proceedings of the NATO Advanced Research Workshop on Coherence in Superconducting Networks, Delft, 1987*, edited by J. E. Mooij and G. B. J. Schön [Physica B **142**, 1–302 (1988)].
[2] D. S. Fisher, M. P. A. Fisher, and D. A. Huse, Phys. Rev. B **43**, 130 (1991).
[3] L. I. Glazman and A. E. Koshelev, Phys. Rev. B **43**, 2835 (1991).
[4] M. A. Moore, Phys. Rev. B **39**,136 (1989); **45**, 7336 (1992).
[5] S. Teitel and C. Jayaprakash, Phys. Rev. Lett. **51**, 1999 (1983).
[6] C. J. Lobb, Physica B **126**, 319 (1984).
[7] J. P. Straley and G. M. Barnett, Phys. Rev. B **48**, 3309 (1993).
[8] W. Y. Shih and D. Stroud, Phys. Rev. B **30**, 6774 (1984); Y.-H. Li and S. Teitel, Phys. Rev. Lett. **65**, 2595 (1990); **67**, 2894 (1991).
[9] S. Teitel and C. Jayaprakash, Phys. Rev. B **27**, 598 (1983); P. Minnhagen, *ibid.* **32**, 7548 (1985); D. B. Nicolaides, J. Phys. A **24**, L231 (1991); J. Lee, J. M. Kosterlitz, and E. Granato, Phys. Rev. B **43**, 11 531 (1991); G. Ramirez-Santiago and J. V. José, Phys. Rev. Lett. **68**, 1224 (1992); Phys. Rev. B **49**, 9567 (1994).
[10] J.-R. Lee, Phys. Rev. B **49**, 3317 (1994).
[11] J.-R. Lee and S. Teitel, Phys. Rev. B **46**, 3247 (1992).
[12] For a recent example see R. Théron, S. E. Korshunov, J. B. Simond, Ch. Leemann, and P. Martinoli, Phys. Rev. Lett. **72**, 562 (1994).
[13] T. C. Halsey, Phys. Rev. Lett. **55**, 1018 (1985); Physica B **152**, 22 (1988).
[14] C. J. Lobb, D. W. Abraham, and M. Tinkham, Phys. Rev. B **27**, 150 (1983).
[15] M. S. Rzchowski, S. P. Benz, M. Tinkham, and C. J. Lobb, Phys. Rev. B **42**, 2041 (1990).
[16] J. P. Straley, Phys. Rev. B **38**, 11225 (1988).
[17] A. Vallat and H. Beck, Phys. Rev. Lett. **68**, 3096 (1992).
[18] For a theoretical arguement consistent with the TJ conjecture for $T_c(f)$, see M. Y. Choi and D. Stroud, Phys. Rev. B **32**, 7532 (1985).
[19] J. M. Kosterlitz and D. J. Thouless, J. Phys. C **6**, 1181 (1973).
[20] B. I. Halperin and D. R. Nelson, Phys. Rev. Lett. **41**, 121 (1978); **41**, 519 (1978); D. R. Nelson and B. I. Halperin, Phys. Rev. B **19**, 2457 (1979).
[21] A. P. Young, Phys. Rev. B **19**, 1855 (1979).
[22] G. S. Grest, P. M. Chaikin, and D. Levine, Phys. Rev. Lett. **60**, 1162 (1988).
[23] J. Villain, J. Phys. (Paris) **36**, 581 (1975).
[24] J. V. José, L. P. Kadanoff, S. Kirkpatrick, and D. R. Nelson, Phys. Rev. B **16**, 1217 (1977); E. Fradkin, B. Huber-

man, and S. Shenker, *ibid.* **18**, 4789 (1978).
[25] P. Minnhagen, Rev. Mod. Phys. **59**, 1001 (1987).
[26] While we expect that the possible thermodynamic states for the cosine and the Villain interactions will be the same, there has been some suggestion that there may be nonuniversal behavior in such models that can result in differing critical exponents for differing interaction potentials; see the work by Lee *et al.* in Ref. 9.
[27] T. Ohta and D. Jasnow, Phys. Rev. B **20**, 130 (1979).
[28] J. Pearl, Appl. Phys. Lett. **5**, 65 (1964).
[29] M. Tinkham, *Introduction to Superconductivity* (R.E. Krieger Co., Malabar, FL, 1980).
[30] B. I. Halperin and D. R. Nelson, J. Low Temp. Phys. **36**, 1165 (1979).
[31] S. Doniach and B. A. Huberman, Phys. Rev. Lett. **42**, 1169 (1979); B. A. Huberman and S. Doniach, *ibid.* **43**, 950 (1979).
[32] D. S. Fisher, Phys. Rev. B **22**, 1190 (1980).
[33] N. D. Mermin and H. Wagner, Phys. Rev. Lett. **17**, 1133 (1966).
[34] L. D. Landau and E. M. Lifshitz, *Theory of Elasticity* (Pergamon, New York, 1970).
[35] For a review, see D. R. Nelson, in *Phase Transitions and Critical Phenomena*, edited by C. Domb and J. L. Lebowitz (Academic, New York, 1983), Vol. 7.
[36] G. S. Grest, Phys. Rev. B **39**, 9267 (1989).
[37] M. Franz and S. Teitel, Phys. Rev. Lett. **73**, 480 (1994).
[38] J. Lee and J. M. Kosterlitz, Phys. Rev. Lett. **65**, 137 (1990).
[39] A. M. Ferrenberg and R. H. Swendsen, Phys. Rev. Lett. **61**, 2635 (1988).
[40] Whether T_c is equal to, or slightly lower than, T_m for the $f = 1/2$ model remains a question of some controversy. See Refs. 9, 10.
[41] M. R. Kolachi and J. P. Straley, Phys. Rev. B **43**, 7651 (1991). See also S. Teitel, Physica B **152**, 30 (1988) and T. C. Halsey, Phys. Rev. B **31**, 5728 (1985) for earlier attempts to find this ground state.
[42] Due to our rescaling of the Coulomb gas temperature by a factor $2\pi J_0$ [see discussion following Eq. (6)], the energy barrier in our units is a factor 2π smaller than the value quoted in Ref. 14 for a Josephson array.
[43] H. S. J. van der Zant, H. A. Rijken, and J. E. Mooij, J. Low Temp. Phys. **79**, 289 (1990).
[44] R. Theron, J.-B. Simond, Ch. Leemann, H. Beck, and P. Martinoli, Phys. Rev. Lett. **71**, 1246 (1993).
[45] Our estimate for the barrier in the honeycomb network follows the calcuation presented in Ref. 14. Note that we have cited here energy barriers as computed for Josephson arrays with a cosine interaction between superconducting nodes, while we have made comparison to transition temperatures T_c and T_m for the Villain interaction between nodes. For the cosine interaction, however, the corresponding transitions will occur at *lower* temperatures than in the Villain case (due to the additional reduction in junction coupling resulting from the vortex–spin-wave interaction which is present in the cosine model). Thus these transitions will be even more obscured by high-energy barriers than our comparison might indicate. Using the same method we have also computed the barriers for the Villain interaction and we have found that for all types of networks these are even much higher (typically by one order of magnitude) than those cited for the cosine model. For example, we have computed $E_b^{\text{Villain}} = 0.517$ for a square network, at low temperature. This large difference comes predominantly from the bond that is crossed by the vortex when climbing to the neighboring site, and it can be easily understood by comparing Villain and cosine potentials. We note also that, although these barriers are important for the dynamics of real networks, they do not effect the equilibration of our simulation; this is because in our Coulomb gas MC, we move vortices in discrete steps to neighboring cells, without the need to climb over the energy barrier. However, had we done typical Metropolis MC in terms of the phases θ_i and the Hamiltonian of Eq. (1), these barriers would cause equilibration problems; this is because when a vortex moves from one cell to its neighbor, the θ_i evolve along a continuous path in phase space that therefore must take the system over the energy barrier separating the two cells.
[46] E. K. F. Dang and B. L. Györffy, Phys. Rev. B **47**, 3290 (1993).
[47] H. S. J. van der Zant, H. A. Rijken, and J. E. Mooij, J. Low Temp. Phys. **82**, 67 (1991).
[48] Ph. Choquard and J. Clerouin, Phys. Rev. Lett. **50**, 2086 (1983); J. M. Caillol, D. Levesque, J. J. Weis, and J. P. Hansen, J. Stat. Phys. **28**, 325 (1982).
[49] E. Brézin, A. Fujita, and S. Hikami, Phys. Rev. Lett. **65**, 1949 (1990); S. Hikami, A. Fujita, and A. I. Larkin, Phys. Rev. B **44**, 10400 (1990).
[50] J. A. O'Neill and M. A. Moore, Phys. Rev. Lett. **69**, 2582 (1992); Phys. Rev. B **48**, 374 (1993).
[51] Z. Tešanović and L. Xing, Phys. Rev. Lett. **67**, 2729 (1991).
[52] Jun Hu and A. H. Macdonald, Phys. Rev. Lett. **71**, 432 (1993).
[53] Y. Kato and N. Nagaosa, Phys. Rev. B **47**, 2932 (1993); **48**, 7383 (1993).
[54] R. Šášik and D. Stroud, Phys. Rev. B **49**, 16074 (1994).
[55] I. F. Herbut and Z. Tešanović, Phys. Rev. Lett. **73**, 484 (1994).
[56] The factor 3/2 in Eq. (8) is included so that the potentials of Eqs. (7) and (8) have the same continuum limit as $a_0 \to 0$; this is desired for modeling a continuous film. For a honeycomb network however, the duality mapping from Eq. (1) leads to Eq. (8) without the factor of 3/2. The transition temperatures we cite for the Coulomb gas on a triangular grid should therefore be scaled by a factor 2/3 to get the corresponding transitions of a honeycomb network, as opposed to a continuous film.
[57] S. A. Hattel and J. M. Wheatley (unpublished).
[58] S. Hattel and J. M. Wheatley, Phys. Rev. B **50**, 16 590 (1994).
[59] P. Martinoli, M. Nsabimana, G. A. Racine, H. Beck, and J. R. Clem, Hel. Phys. Acta **55**, 655 (1982).

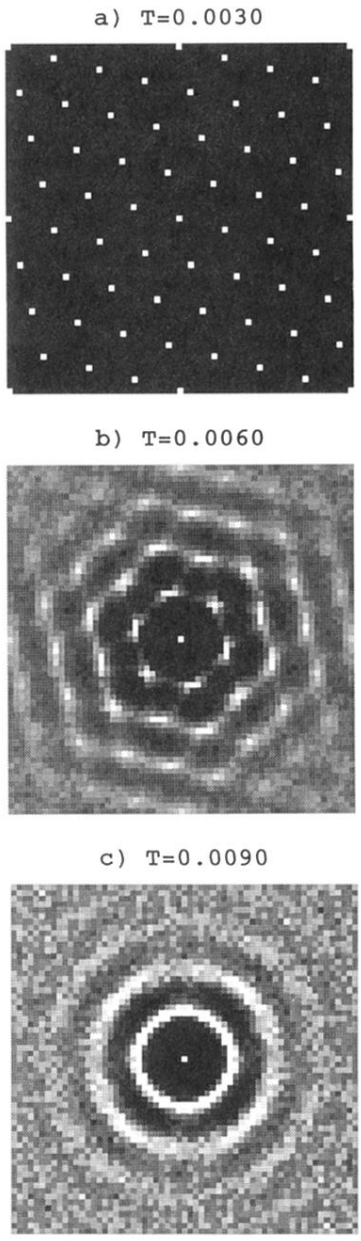

FIG. 16. Melting of a nearly triangular vortex lattice on the square grid. Intensity plots of $S(\mathbf{k})$ for $f = 1/60$, $L = 60$, and several temperatures: (a) $T = 0.003$ in the pinned solid, (b) $T = 0.006$ floating solid, (c) $T = 0.009$ in the liquid.

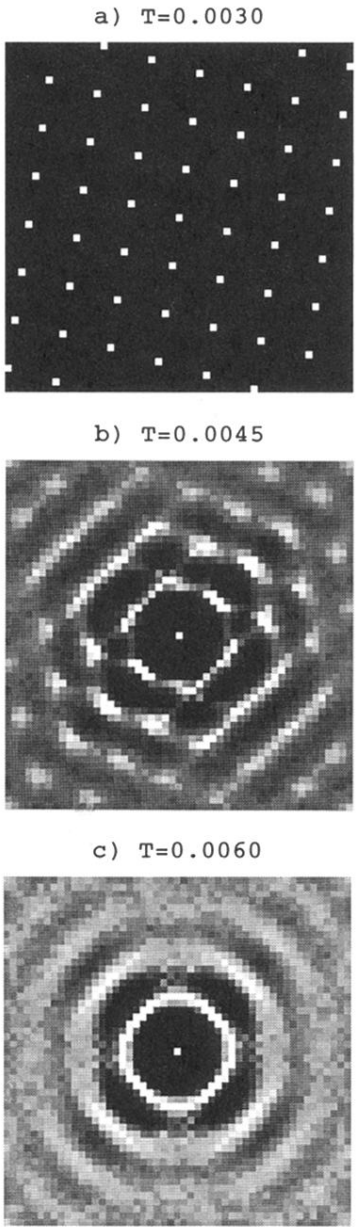

FIG. 19. Melting of a nearly square vortex lattice on the square grid. Intensity plots of $S(\mathbf{k})$ for $f = 1/51$, $L = 51$, and several temperatures: (a) $T = 0.003$ in the pinned solid, (b) $T = 0.0045$ in the floating solid, (c) $T = 0.006$ in the liquid.

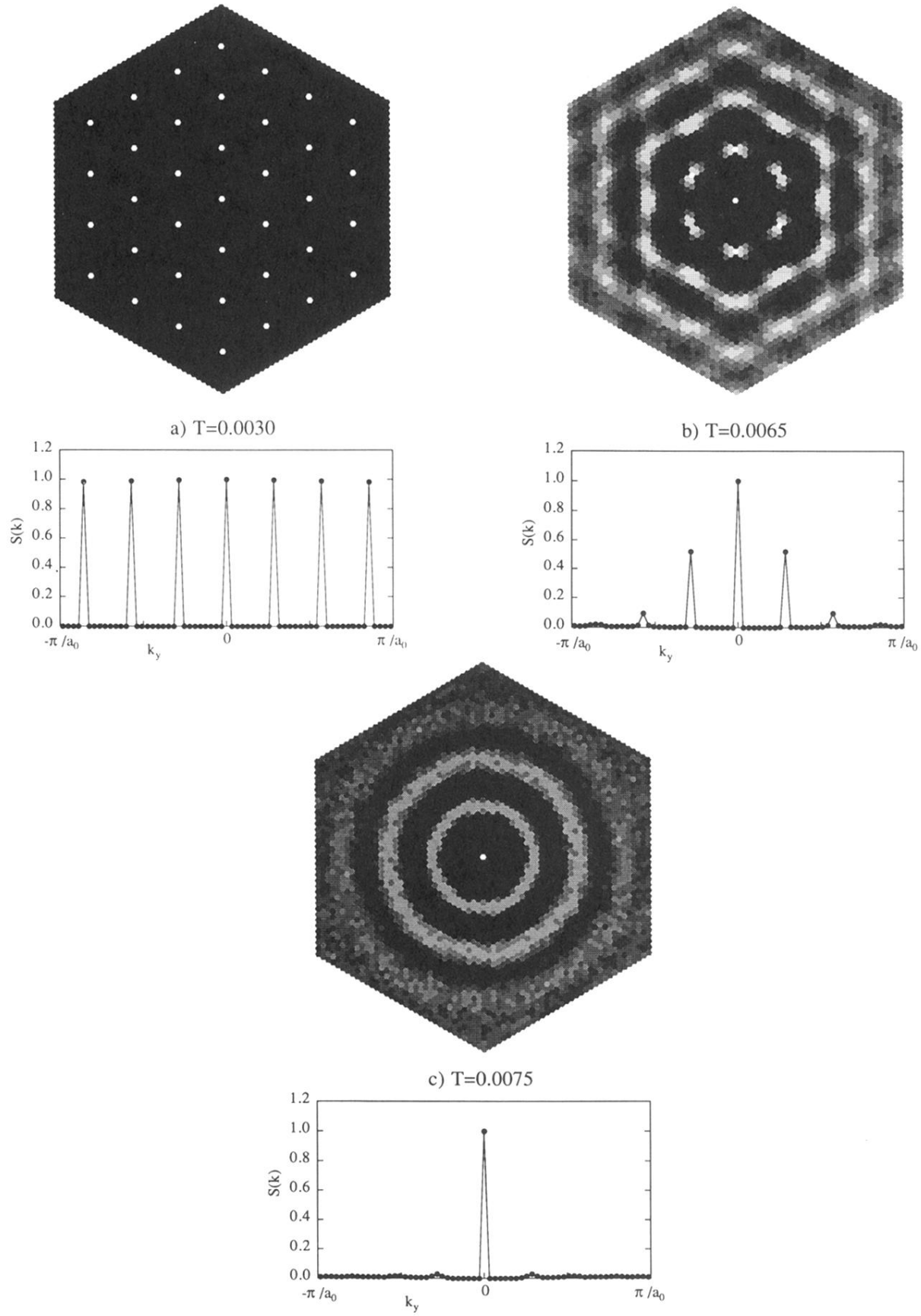

FIG. 2. Structure function $S(\mathbf{k})$ in the first Brillouin zone (upper portion of the figure) and the profile of the peak heights along the vertical symmetry axis k_y (lower portion), for $f = 1/49$ and $N_c = 63$, and three different temperatures T: (a) $T = 0.003$, just below T_c, in the "pinned solid" phase, (b) $T = 0.0065$, just below T_m, in the "floating solid" phase, (c) $T = 0.0075$, just above T_m, in the liquid. Intensities in the density plots are plotted nonlinearly to enhance features.

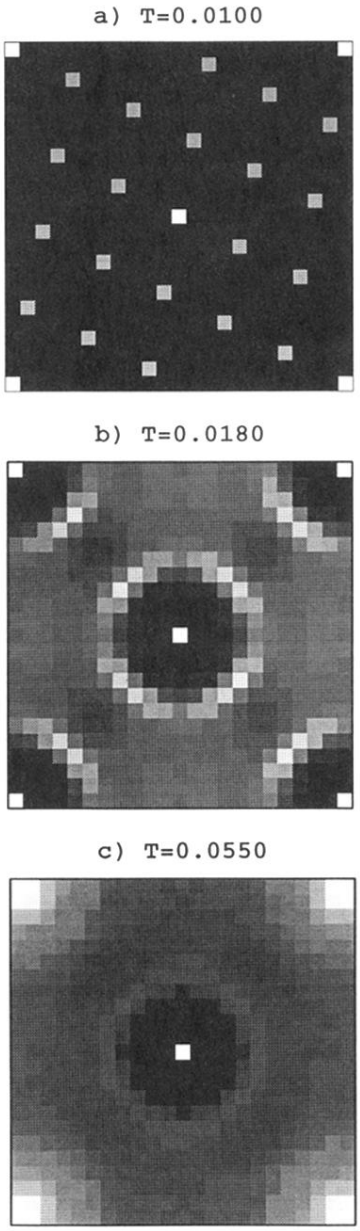

FIG. 21. Melting of $f = 5/11$ for $L = 22$. $S(\mathbf{k})$ is shown for (a) $T = 0.010$ in the pinned defect solid, (b) $T = 0.018$ in the defect liquid, (c) $T = 0.055$ in the completely disordered high-temperature phase.

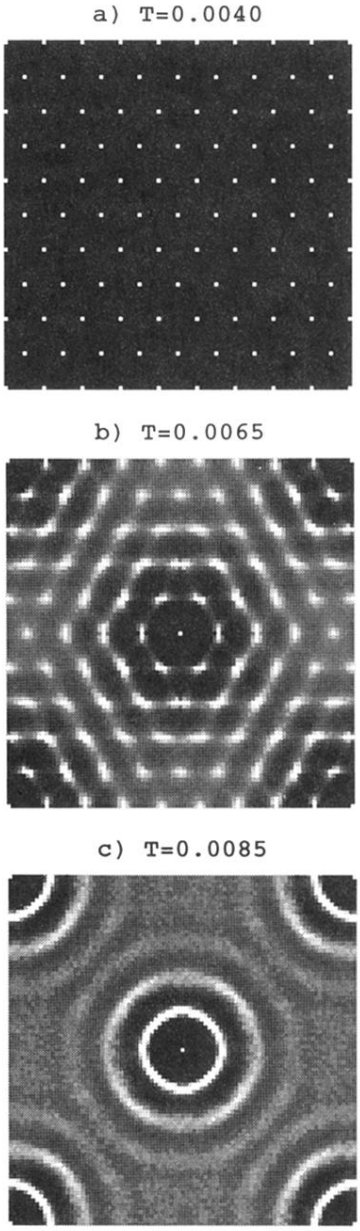

FIG. 24. Melting of the defect superlattice for $f = 22/45$ and $L = 90$. Intensity plot of $S(\mathbf{k})$ for (a) $T = 0.0040$ in the pinned defect solid, (b) $T = 0.0065$ in the defect floating solid, (c) $T = 0.0085$ in the defect liquid. Intensities at $(\pm\pi/a_0, \pm\pi/a_0)$ and $(0,0)$, which arise from the fixed staggered background, have been substracted for the sake of clarity.